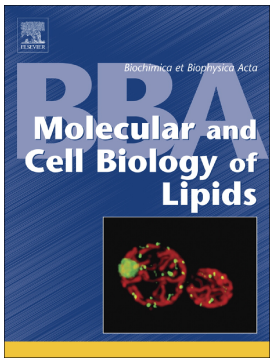

Turnover of bile acids in liver, serum and caecal content by high-fat diet feeding affects hepatic steatosis in rats

Yingyue Tang, Jingyi Zhang, Jing Li, Xiaohong Lei, Dongke Xu, Yang Wang, Chunmin Li, Xiaobo Li, Yimin Mao

PII: S1388-1981(19)30090-3
DOI: https://doi.org/10.1016/j.bbalip.2019.05.016
Reference: BBAMCB 58472

To appear in: *BBA - Molecular and Cell Biology of Lipids*

Received date: 27 January 2019
Revised date: 22 May 2019
Accepted date: 30 May 2019

Please cite this article as: Y. Tang, J. Zhang, J. Li, et al., Turnover of bile acids in liver, serum and caecal content by high-fat diet feeding affects hepatic steatosis in rats, BBA - Molecular and Cell Biology of Lipids, https://doi.org/10.1016/j.bbalip.2019.05.016

Turnover of bile acids in liver, serum and caecal content by high-fat diet feeding affects hepatic steatosis in rats

Yingyue Tang[1,*], Jingyi Zhang[1,*], Jing Li[1,*], Xiaohong Lei[1], Dongke Xu[2], Yang Wang[3], Chunmin Li[1], Xiaobo Li[2,§], Yimin Mao[1,§]

[1]Division of Gastroenterology and Hepatology, Key Laboratory of Gastroenterology and Hepatology, Ministry of Health, Renji Hospital, School of Medicine, Shanghai Jiao Tong University, Shanghai Institute of Digestive Disease, Shanghai, China. [2]Department of Physiology and Pathophysiology, School of Basic Medical Sciences, Fudan University, Shanghai, China.

[3]Shanghai University of Traditional Chinese Medicine, Shanghai, China.

*Yingyue Tang, Jingyi Zhang and Jing Li contributed equally.

[§]Corresponding authors:
Yimin Mao;

Division of Gastroenterology and Hepatology, Key Laboratory of Gastroenterology and Hepatology, Ministry of Health, Renji Hospital, School of Medicine, Shanghai Jiao Tong University, Shanghai Institute of Digestive Disease, Shanghai, China. E-mail addresses: maoym11968@163.com

Xiaobo Li;

Department of Physiology and Pathophysiology, School of Basic Medical Sciences, Fudan University, Shanghai, China. E-mail addresses: xbli@fudan.edu.cn

Abstract

Background: Bile acids (BAs) participate in lipid absorption and serve as metabolic regulatory factors in gut-liver communication. To date, there are no studies on the systemic patterns of BAs in the serum, liver, and gut in the same non-alcoholic fatty

liver disease (NAFLD) model.

Methods: A targeted metabolomics approach and 16S rRNA sequencing were used to identify the profile of BAs and connection between BAs and microbiota. The role and mechanism of altered BAs on hepatic steatosis were investigated.

Findings: In the liver, the composition of taurocholic acid (TCA) was increased, but taurohyodeoxycholic acid (THDCA) and ursodeoxycholic acid (UDCA) were decreased. In the gut, the deconjugated form of TCA (cholic acid (CA)) was increased, while the deconjugated forms of THDCA (α-hyodeoxycholic acid (HDCA)) and ω-muricholic acid (ωMCA) were decreased. In the serum, the composition of TCA was increased, while both HDCA and THDCA were decreased. THDCA induced the gene expression of apolipoprotein, bile secretion-related proteins, and cytochrome P450 family but suppressed inflammatory response genes expression in steatotic hepatocytes by RNAseq analysis. THDCA ameliorated neutral lipid accumulation and improved insulin sensitivity in primary rat hepatocytes. The decreased HDCA level correlated with the level of Bacteroidetes, while the level of CA correlated with the levels of Firmicutes and Verrucomicrobia but correlated inversely with Bacteroidetes.

Conclusion: BAs profiles in the serum, liver and caecal content were altered in a rat NAFLD model, which may affect hepatic lipid accumulation and correlate with gut dysbiosis.

Keywords: Non-alcoholic fatty liver disease; Bile acid; Gut microbiota; TCA; THDCA

Abbreviations:

BAs, Bile acids; NAFLD, non-alcoholic fatty liver disease; TCA, taurocholic acid; THDCA, taurohyodeoxycholic acid; UDCA, ursodeoxycholic acid; CA, cholic acid; HDCA, α-hyodeoxycholic acid; ωMCA, ω-muricholic acid; NASH, non-alcoholic steatohepatitis; VLDL, very low density lipoprotein; FXR, farnesoid X receptor; TGR5, G protein couple receptor 5; BSH, bile salt hydrolase; ASBT, apical sodium-dependent BA transporter; GCDCA, glycochenodeoxycholic acid; DCA, deoxycholic acid; TCDCA, taurochenodeoxycholic acid; ALT, alanine

aminotransferase; AST, aspartate aminotransferase; TG, triglyceride; TC, total cholesterol; HDL-C, high-density lipoprotein cholesterol; LDL-C, low-density lipoprotein cholesterol; GLU, fasting blood glucose; H&E, haematoxylin and eosin; βDCA, 3β-deoxycholic acid; 6-ketoLCA, 6-ketolithocholic acid; TαMCA, tauro α-muricholic acid; TβMCA, tauro β-muricholic acid; TLCA, taurolithocholic acid; TDCA, taurodeoxycholic acid; TωMCA, tauro ω-muricholic acid; NorDCA, 23-nordeoxycholic acid; LCA, lithocholic acid; βCDCA, 3β-chenodeoxycholic acid; CDCA, chenodeoxycholic acid; GUDCA, glycoursodeoxycholic acid; GCA, glycocholic acid; ACA, allocholic acid; muroCA, murocholic acid; PCOA, principle coordinate analysis; TUDCA, tauroursodeoxycholic acid;

1. Introduction

Almost 30% of the global population is affected by non-alcoholic fatty liver disease (NAFLD), which accompanies the increasing prevalence of other metabolic abnormalities, including type 2 diabetes, obesity, and cardiovascular disease [1-3]. The spectrum of NAFLD ranges from simple steatosis to non-alcoholic steatohepatitis (NASH) with the development of fibrosis and cirrhosis [4]. NAFLD derives from the accumulation of different lipid species within hepatocytes, which is driven by insulin resistance from energy imbalance, such as excessive free fatty acid delivery to the liver, increased de novo lipogenesis, inadequate increases in very low density lipoprotein (VLDL) secretion, beta-oxidation and bile acid (BA) excretion [5-7]. Although the liver is the master hub that regulates metabolic processes, multiple organs, including adipose tissue, pancreas, muscle and gut, also participates in the progression of NAFLD. Recent studies have shown that changes in the microbiota have a prominent role in NAFLD pathogenesis [8]. The inter-organ communication between the liver and gut is orchestrated by such metabolites as glucose, fatty acid, sterols and BAs [9, 10].

In the liver, primary BAs are biosynthesized from cholesterol and the conjugation with either taurine or glycine makes BAs less hydrophobic and lower toxicity [11]. After biliary secretion, primary BAs are extensively metabolized by the microbiota into secondary BAs, which are more hydrophobic and thus more cytotoxic; then, the secondary BAs are reabsorbed and recirculated through enterohepatic circulation [12, 13]. Exposure to relatively more hydrophobic BAs

(lithocholic acid (LCA), glycochenodeoxycholic acid (GCDCA), deoxycholic acid (DCA) and chenodeoxycholic acid (CDCA)) would induce mitochondrial function disorder and endoplasmic reticulum stress and stimulate inflammatory mediators, resulting in the necrosis and apoptosis of hepatocytes [14]. However, hydrophilic BAs, such as ursodeoxycholic acid (UDCA) and glycoursodeoxycholic acid (GUDCA), have hepatoprotective as well as choleretic effects. With the help of active transport processes, the BA enterohepatic circulation participates in several hepatic and gastrointestinal physiological functions including bile flow, cholesterol solubilization and excretion, toxic substance clearance, intestinal absorption of lipophilic nutrients, and metabolic and antimicrobial effects [15].

BAs not only play important roles in the emulsification and absorption of dietary fats and vitamins from the small intestine but also serve as potent signalling molecules. BA signalling is important in the regulation of BA metabolism itself, cholesterol secretion, cholesterol gallstone formation, glucose, lipid, and energy metabolism. BA signalling pathways by the nuclear receptor farnesoid X receptor (FXR), G protein couple receptor 5 (TGR5) and other nuclear receptors have been identified and well-characterized as mediators of insulin resistance, obesity, lipid metabolism and systemic metabolic processes [16, 17]. The homeostasis of BA composition is not only controlled by the normal function of hepatocytes, the biliary system and ileal enterocytes but also by the appropriate interaction between BAs and the gut microbiota [12, 14, 18]. BAs could influence the gut microbiota composition by shaping the host's intestinal immunity and some intrinsic antimicrobial properties [19, 20]. In turn, alterations in the composition of the microbiota affect BA synthesis and uptake [21]. For example, BAs are directly deconjugated by gut bacteria, such as *Bacteroides*, *Clostridium*, and *Eubacterium* with bile salt hydrolase (BSH) activity [17]. In addition, modulating apical sodium-dependent BA transporter (ASBT) and the signalling properties of BAs by microbial enzymatic activities in the small intestine would prevent active reuptake of BAs [22].

With the development of both non-targeted and targeted metabolomics in recent decades, quantitative analyses can test more than 70 types of BA metabolites. Some studies reported the composition or changes in BAs of the serum, liver or faeces in NAFLD rodent models or patients [4, 23]. García-Cañaveras et al used an untargeted metabolomic method to discover four elevated BAs, including GCDCA,

glycochenodeoxycholate-3-sulfate, taurochenodeoxycholic acid (TCDCA) and taurocholic acid (TCA) in human steatotic liver [24]. Compared with healthy donors, the significant alterations in BAs, including primary and secondary BAs in the blood, were found in NASH patients but not NAFL patients [25, 26]. Mouzaki et al used a quantitative faecal BA method and found a significant increase in primary BAs and total BAs in NAFL patients compared to healthy donors [27]. Zheng et al found a robust and significant increase in the intestinal BA pool including 42 quantified BAs within 12 h of high-fat diet treatment in mice [18]. Since the BA pool is coordinately regulated by the liver and gut, a comprehensive understanding of the metabolism of BAs in the overall BA circulation system, including the liver, gut and serum, is of great importance. To date, there have been no reports on the systemic patterns of BAs in the serum, liver, and caecal content in the same NAFLD model.

Our present study utilized a targeted metabolomics approach to identify the profile of BAs in the serum, liver, and caecal content and used 16S rRNA in the caecal content microbiome to elucidate the connection between BAs and the microbiota in NAFLD and investigated the role and potential mechanism of altered BAs in the liver on hepatic steatosis.

2. Materials and Methods

2.1 Animal studies and sample collection

Ten six-week-old male Sprague–Dawley rats were purchased from the Shanghai Experimental Animal Centre of the Chinese Academy Sciences (Shanghai, China). All animal experiments were performed following the National Institutes of Health Guidelines for the Care and Use of Laboratory Animals and were permitted by the Institutional Animal Care and Use Committee of RenJi Hospital, School of Medicine, Shanghai Jiao Tong University. Rats were fed a standard diet with 1 week of acclimatization and later randomly assigned to the two groups. The Control group received a normal diet (10 kcal%), while the NAFLD group was fed a high-fat diet (D12492, 60 kcal%, Research Diets, New Brunswick, NJ, USA) for eighteen weeks to establish the NAFLD model. Rats were fed the diets and water *ad libitum* and housed in a pathogen-free, temperature and humidity controlled environment with a 12 h light/12 h dark cycle. Body weight and food intake were monitored weekly for 18

weeks. All rats were fasted overnight before sacrifice, and then blood samples were collected from the retinal venous plexus. The blood was centrifuged at 3,000 g for 15 min at 4 °C for serum collection. Parts of the liver were fixed in 4% formaldehyde overnight for histological examination or snap-frozen for later analysis. Other livers, stool samples and caecal content were carefully dissected and kept in liquid nitrogen before storage at −80 °C.

2.2 Biochemical index and histological analysis

The analysis of serum alanine aminotransferase (ALT), aspartate aminotransferase (AST), triglyceride (TG), total cholesterol (TC), high-density lipoprotein cholesterol (HDL-C), low-density lipoprotein cholesterol (LDL-C) and fasting blood glucose (GLU) were measured using an automatic biochemical analyser (Siemens Advia 1800, Siemens Healthcare Diagnostics, Tarrytown, NY, USA). Paraffinized and frozen liver sections were stained with haematoxylin and eosin (H&E) and oil Red O, respectively.

2.3 BA metabolite profile assessment

The BAs from the serum, liver, caecal content were quantitatively measured by Metabo-Profile Inc. (Shanghai, China) according to a previously reported protocol [18, 28, 29]. BA analysis was performed with an ACQUITY BEH C18 column (1.7 mm,100 mm, 32.1 mm internal dimensions) (Waters Corp., Milford, MA, USA). One standard calibration solution at 10 different concentration levels contains 73 standards and the QC was tested every 12 samples. The peak annotation and quantitation were performed by TargetLynx application manager (Waters Corp., Milford, MA, USA). For details, see Methods in the Supporting Information.

2.4 Gut microbe 16S rRNA sequencing

Microbial DNA was extracted from rat caecal content and stool samples using the E.Z.N.A.® Soil DNA Kit (Omega Bio-tek, Norcross, GA, USA) according to the manufacturer's protocols. The final DNA concentration and purification were determined using a NanoDrop 2000 UV-vis spectrophotometer (Thermo Scientific, Wilmington, USA), and DNA quality was checked by 1% agarose gel electrophoresis. The V3-V4 hypervariable regions of the bacterial 16S rRNA gene were amplified with primers 338F (5 '- ACTCCTACGGGAGGCAGCAG-3') and 806R

(5 '-GGACTACHVGGGTWTCTAAT-3') with a thermocycler PCR system (GeneAmp 9700, ABI, USA). The PCR reactions were as follows: 3 min of denaturation at 95 ℃, 27 cycles of 30 s at 95 ℃, 30 s for annealing at 55 ℃, and 45 s for elongation at 72 ℃, and a final extension at 72 ℃ for 10 min. PCR reactions were performed in a 20 μL mixture containing 4 μL of 5×FastPfu Buffer, 2 μL of 2.5 mM dNTPs, 0.8 μL of each primer (5 μM), 0.4 μL of FastPfu Polymerase and 10 ng of template DNA. The PCR products were extracted from a 2% agarose gel and further purified using the AxyPrep DNA Gel Extraction Kit (Axygen Biosciences, Union City, CA, USA) and quantified using QuantiFluor™-ST (Promega, Madison, WI, USA) according to the manufacturer's protocol. Purified amplicons were pooled in equimolar and paired-end sequenced (2×300) on an Illumina MiSeq platform (Illumina, San Diego, CA, USA) according to the standard protocols by Majorbio Bio-Pharm Technology Co. Ltd. (Shanghai, China). Raw fastq files were quality-filtered by Trimmomatic and merged by FLASH with the following criteria: (i) The reads were truncated at any site receiving an average quality score <20 over a 50 bp sliding window. (ii) Sequences with an overlap longer than 10 bp were merged according to their overlap with a mismatch of no more than 2 bp. (iii) Sequences of each sample were separated according to barcodes (exactly matching) and primers (allowing 2 nucleotide mismatching), while reads containing ambiguous bases were removed. Operational taxonomic units (OTUs) were clustered with 97% similarity cut-off using UPARSE (version 7.1 http://drive5.com/uparse/) with a novel 'greedy' algorithm that performs chimaera filtering and OTU clustering simultaneously. The taxonomy of each 16S rRNA gene sequence was analysed using an RDP Classifier algorithm (http://rdp.cme.msu.edu/) against the Silva (SSU123) 16S rRNA database using a confidence threshold of 70%.

2.5 Primary Rat hepatocyte isolation

Hepatocytes were isolated from rats by a two-step collagenase perfusion according to a previous method [30]. The digested liver sections were filtered through a 70-μm nylon mesh. Rat hepatocytes were collected after centrifugation at 50×g for 5 min. The cells were washed twice with DMEM and then resuspended in culture medium (William's medium E, 10% FBS). Trypan Blue exclusion yielded cell viability greater than 85%. The cells were plated in collagen I coated six-well plates with William's E medium supplemented with 10% FBS, penicillin (100 U/ml) and streptomycin (100 mg/ml). Cells were cultured in a humidified incubator at 37℃ and

5% CO_2. Experiments were started at 4 h after the isolation of hepatocytes. The medium was replaced with a fresh medium with the addition of oleic acid and palmitic acid at a ratio of 2:1 at a concentration of 0.25 mmol/L; BSA was used as a control. After 48 h of incubation, the culture medium was removed, cells were washed with PBS twice and further cultured in medium with or without 10 μM Z-guggulsterone (Selleck Chemicals, Texas, USA) for 2 h before the addition of TCA (Sigma Aldrich, St. Louis, MO, USA) at 62.5 μM, 125 μM, 250 μM, 500 μM, and 1000 μM, and taurohyodeoxycholic acid (THDCA) (Shanghai ZZBio CO LTD, Shanghai, China) at 15 μM, 30 μM, 62.5 μM, 125 μM, and 250 μM. After 24 h, cells were washed with PBS before RNA isolation and Oil Red O staining. At the same time, after this preincubation, the cells with OAPA or THDCA (250 μM) were treated with 10 μg/ml insulin for 0, 20, and 40 min and then collected for immunoblot analysis.

2.6 RNA-Seq analysis

Total RNA was isolated using TRIzol Reagent (Invitrogen, Carlsbad, CA, USA) according to the manufacturer's instructions. The cDNA Library preparation was done using the RNA-Seq Sample Prep Kit (Illumina) according to the manufacturer's instructions. For the QC step, an Agilent 2100 Bioanalyzer and an ABI StepOnePlus Real-Time PCR System were used to qualify and quantify the sample library. Each cDNA library was amplified once before sequencing. Sequencing was performed on an Illumina HiSeq X Ten at Biotecan Co., Ltd. (Shanghai, China). The RNA-Seq data were analysed as previously described [31, 32]. DAVID (http://david.abcc.ncifcrf.gov/home.jsp) functional annotation cluster analysis was performed on the list of differentially expressed genes (over 1.5-fold and $P<0.05$). The gene ontology (GO) biological process (BP) terms were used to categorize the enriched biological themes in the list of differentially expressed genes in DAVID.

2.7 Quantitative real-time PCR

Total RNA was extracted from rat liver tissues and cells using TRIzol reagent, and reverse transcription was performed using PrimeScript RT Reagent Kit (Takara, Shiga, Japan), according to the manufacturer’s instructions. Quantitative PCR was performed with a SYBR Green PCR kit (Takara, Shiga, Japan) using GAPDH as an internal standard. The primers used for gene expression analysis are shown in Supplementary Table 1.

2.8 Oil red O staining

Cells were stained with oil red O solution (Goodbio Technology, Wuhan, China). Briefly, cells were washed three times with PBS and fixed with 4% formalin. After fixation, cells were incubated with 0.5% oil red O solution for 1 h at room temperature. Images were obtained using a microscope (Olympus, Japan).

2.9 Western blot analysis

Proteins from primary rat hepatocytes were extracted in RIPA buffer (Beyotime, Shanghai, China). Total protein samples of 100 μg each were separated on a 10% SDS-PAGE and electro-transferred to PVDF membranes. After blocking with 5% BSA in TBST for 1 h at room temperature, the membranes were incubated with antibodies against phospho-Akt Ser473 (Cell signalling technology, MA, USA), total-AKT (Cell signalling technology, MA, USA), and beta-actin (Proteintech, IL, USA) overnight at 4℃. The protein signals were visualized using the ECL Western Blotting Kit (Bio-Rad, Hercules, Calif., USA).

2.10 Cell transfection and dual-luciferase assay

The BRL-3A rat hepatocytes were purchased from the Cell Bank of the Chinese Academy of Sciences (Shanghai, China). Cells were cultivated in high-glucose DMEM supplemented with 10% FBS and 100 U/ml penicillin-streptomycin at 37°C in an atmosphere containing 5% CO_2. pGMFXR-Lu (Genomeditech, Shanghai, China) and pRL vector (Renilla luciferase control reporter vector) were co-transfected into BRL-3A cells by using Lipofectamine 3000 (Invitrogen) for 24 h; then, cells were incubated with THDCA or PBS for another 24 h, and luciferase activities were measured by a dual-luciferase reporter kit (Beyotime, China).

2.11 Statistical analysis

All of the physiological, biochemical, BA, and microbiota data were collected from five individuals per group as biological replicates. Taxonomy abundance at different ranks was normalized to the summation by each sample. The BA data generated from the UPLC-TQMS analysis were imported to the Simca-P 13.0 software package (Umetrics, Umea, Sweden) for multivariate statistical analysis. Mann–Whitney U tests and Spearman correlation were performed using SPSS 13.0 software (IBM Corp, Armonk, NY, USA). The statistically significant p values were adjusted using a false discovery rate of 0.05. Spearman correlation analysis was used

to evaluate the interactions between gut microbiota and BA levels, giving a value ranging from 1.0 (maximum positive correlation) to -1 (maximum negative correlation) and 0 (no correlation). All statistical graphs were made using GraphPad Prism (version 6.0; GraphPad Software, San Diego, USA).

3. Results

3.1 Concentrations of BA species in the serum, liver and caecal content were altered in the NAFLD rat model

To study chronic high-fat diet induced hepatic steatosis and changes in BAs, we fed rats with a high-fat diet for 18 weeks. The NAFLD group exhibited increased body weight and liver index (liver to body weight ratio) (Fig. S1A, Fig. S1B). The HE and oil Red O of liver samples from the NAFLD group displayed steatosis or microvesicular fatty degeneration (Fig. S1C, Fig. S1D, Fig. S1E, Fig. S1F). The levels of ALT and AST in the serum significantly increased in the NAFLD group (Fig. S1G). The serum TC, LDL-C and glucose increased significantly and serum HDL-C decreased significantly (Fig. S1H).

BAs from the serum, liver, and caecal content were analysed using UPLC-MS/MS. From the serum samples, the NAFLD group demonstrated significantly increased TCA and decreased α-hyodeoxycholic acid (HDCA), THDCA, 3β-deoxycholic acid (βDCA), and 6-ketolithocholic acid (6-ketoLCA) compared to the Control group (Fig. 1A). In the liver, only one tauro-conjugated BA, TCA, was significantly increased. However, 10 BAs from the NAFLD group were significantly decreased in the liver, including 4 tauro-conjugated BA species including taurolithocholic acid (TLCA), THDCA, taurodeoxycholic acid (TDCA) and tauro ω-muricholic acid (TωMCA). Furthermore, βDCA, HDCA, 6-ketoLCA, 23-nordeoxycholic acid (NorDCA), LCA and 3β-chenodeoxycholic acid (βCDCA) showed lower levels in the NAFLD group (Fig. 1B). In the caecal content, primary BAs including cholic acid (CA) and chenodeoxycholic acid (CDCA) were significantly increased. In addition, glycine-conjugated species, such as GUDCA, glycocholic acid (GCA) and allocholic acid (ACA), were significantly increased, while HDCA, murocholic acid (muroCA), NorCA and ω-muricholic acid (ωMCA) were decreased in the NAFLD group (Fig. 1C).

3.2 Composition of BA species in the serum, liver and caecal content were altered in the NAFLD rat model

We calculated the percentage of the concentration of each BA to the concentration of the sum of all BA species. As a result, in the serum, the NAFLD group had a decreased ratio of HDCA of 9.54%, which accounted for 32.85% in the Control group. The TCA proportion rose to 19.77% compared to the Control group at 3.75%, while the percentage of muroCA, 6-ketoLCA, βDCA and ωMCA significantly decreased after HFD feeding in the serum (Fig. 2A, Fig. 2B). As a high proportional component of the BA pool in the liver, the TCA proportion increased from 40.80% to 61.90% with HFD treatment, the result of which was consistent with its increasing trend in the serum. However, the THDCA proportion decreased from 13.95% to 3.06%. Most BA proportions decreased with HFD treatment, including tauro-conjugated species such as TωMCA, TDCA, TLCA, βDCA, 6-ketoLCA, HDCA, LCA, NorDCA, muroCA, 3β-chenodeoxycholic acid (βCDCA), and UDCA (Fig. 2C, Fig. 2D). Caecal results showed a significantly elevated proportion of CA from 3.03% to 26.11% and other elevated BAs including GCA, CDCA, 3-dehydrocholic acid (3-DHCA), ACA, and NorCA, and a diminished proportion of ωMCA, HDCA, and muroCA with HFD treatment (Fig. 2E, Fig. 2F).

3.3 Effects of THDCA and TCA on hepatic steatosis in vitro

Based on the above data, as the two most prevalent components of the BA pool in liver, the concentrations of TCA and THDCA in the liver were dramatically changed by high-fat diet feeding. The TCA level increased significantly while the THDCA level decreased significantly. In addition, in the caecal content and serum samples, TCA and THDCA, or their related deconjugation species, paralleled the changes observed in the liver samples. RNA sequencing was used to study the transcriptional profile alterations of steatotic primary rat hepatocytes upon TCA and THDCA treatment. The cluster map illustrated that the concentrations of THDCA and TCA changed significantly in response to OAPA treatment (Fig. 3A). As shown in Fig. 3B, there were a total of 324 changed genes (over 1.5-fold, $p<0.05$) in the OAPA group compared with the genes in the BSA group; among these genes, 226 were upregulated and 96 were downregulated. Compared with OAPA-treated cells, 190 genes were upregulated (over 1.5-fold, $p < 0.05$) and 145 genes were downregulated (over 1.5-fold, $p<0.05$) in the THDCA group, while there were 89

upregulated genes and 69 downregulated genes in the TCA group (Fig. 3C, 3D). The upregulated and downregulated genes were pooled, and gene ontology (GO) analysis was performed using the DAVID default parameters. As shown in Fig. 3E, the 190 genes that were upregulated in the THDCA group, compared to their expression in the OAPA group, were mainly enriched in areas such as "lipid metabolic process", "regulation of transport", and "fatty acid derivative metabolic process". As shown in Fig. 3F, the genes downregulated in the THDCA group compared to their expression in the OAPA group were mainly enriched in processes such as "regulation of cell proliferation", "cell differentiation", and "regulation of transport". Therefore, THDCA treatment might improve lipid processing and BA transportation. THDCA treatment upregulated the transcription of the apolipoprotein family (Apoa1, Apoa4, Apob), bile secretion (Baat, Abcc3, Ephx1), insulin-like growth factor binding protein (Igfbp1, Igfbp4) and the cytochrome P450 family (Cyp1a1, Cyp2a1), while it suppressed the expression of inflammatory response (Cxcl12, Cxcl3) and LPS response genes (Wnt7a, Nppb) (Fig. 3G). Oil Red O staining revealed that THDCA (250 μM) treatment significantly ameliorated neutral lipid accumulation in OAPA-treated hepatocytes (Fig. 3H). Following stimulation with insulin, THDCA (250 μM) could elevate the level of phospho-Akt, resulting in improvements in the insulin signalling pathway (Fig. 3I). Raw data of RNA sequencing were deposited at SRA database of NCBI with the accession number SRP199028.

3.4 THDCA ameliorated hepatic steatosis by activating FXR in vitro

As shown above, many of the genes regulated by THDCA are FXR's downstream genes. The mRNA level of FXR was upregulated in the steatotic liver compared with the normal liver (Fig. 4A). We observed that THDCA (250 μM) treatment increased the activity of FXR reporter activity in BRL-3A cells, indicating that THDCA was able to activate FXR (Fig. 4B). Moreover, Oil Red O staining showed that THDCA treatment significantly ameliorated neutral lipid accumulation in OAPA-treated BRL-3A cells, and the neutral lipid accumulation was markedly increased in response to the combination treatment of THDCA and Z-guggulsterone (Fig. 4C). Furthermore, compared with the results of the OAPA group, THDCA treatment significantly increased the mRNA expression of FXR's downstream genes including Ppargc1a, NTCP, Fkp5 and Lpin1, and this increased expression was

attenuated by the FXR antagonist Z-guggulsterone (Fig. 4D). Similar results were seen in rat primary hepatocytes by qRT-PCR (Fig. 4E). The mRNA levels of FXR and FXR's downstream genes (BSEP, CYP2c22, NTCP, Lpin1, etc.) were dose-dependently increased by THDCA, whose effects were more obvious than those of TCA. In the presence of Z-guggulsterone, the promoting effects of THDCA and TCA were attenuated.

3.5 Alteration of gut microbiome composition in response to HFD feeding

As BAs are closely related to the gut microbiota, we next performed 16S rRNA gene sequencing with the caecal content samples. An unweighted principle coordinate analysis (PCOA) revealed that the gut microbiota structure changed significantly in response to HFD feeding. HFD-related differences were mainly observed along the first principal coordinate (PCoA1), which accounted for the largest proportion (52.1%) of total variation (Fig. 5A), while PCoA2 made up 20.08% of the total variation. Furthermore, the hierarchical clustering tree based on OTU level showed the gut microbiota structure of all samples (Fig. 5B).

At the phylum level, 13 different phyla were identified in both groups, which were dominated by members of the Firmicutes, Bacteroidetes and Proteobacteria phyla. By comparing the taxonomic profiles at the phylum level, the NAFLD group was characterized by a significantly elevated enrichment of Firmicutes at 87.95% abundance compared to 61.60% in the Control group. However, the Control group had a higher abundance of Bacteroidetes (30.35% compared to 3.67% in the NAFLD group (Fig. 5C, 5D)). The results could indicate the NAFLD could increase the ratio of Firmicutes to Bacteroidetes. After HFD treatment, the Verrucomicrobia abundance increased significantly from 0.14% to 3.85%. Moreover, there were reductions in the prevalence of the Cyanobacteria, Saccharibacteria and Elusimicrobia phyla in the NAFLD group versus the Control group.

At the genus level, the taxonomic analysis revealed the presence of 153 genera, 74 of which exhibited significant changes between the two groups. The results were similar to those presented at the phylum level. The abundance of *norank_f__Bacteroidales_S24-7_group*, *Alloprevotella*, *Prevotellaceae_Ga6A1_group*, *Prevotellaceae_NK3B31_group*, *Prevotella_9*, *Alistipes*, *Prevotellaceae_UCG-001*, *Butyricimonas*, *unclassified_f_Prevotellaceae*

and *unclassified_f__Porphyromonadaceae* belonging to the phylum *Bacteroidetes* also decreased significantly in the NAFLD model. Consistent with the change in the *Firmicutes* phylum, the abundance of *Phascolarctobacterium*, *[Eubacterium]_fissicatena_group*, *Terrisporobacter*, *[Ruminococcus]_torques_group*, *Erysipelatoclostridium*, *Lachnospiraceae_UCG-010*, *Faecalitalea*, *Candidatus_Stoquefichus*, *Staphylococcus*, *Enterococcus*, *Blautia*, *unclassifiedoClostridiales*, *Granulicatella*, *[Eubacterium]_nodatum_group*, *Streptococcus*, *Lactococcus*, *Christensenellaceae_R-7_group*, *[Ruminococcus]_gauvreauii_group*, *Family_XIII_AD3011_group* and *Candidatus_Soleaferrea* increased significantly, while the abundance of *Akkermansia* from the phylum *Verrucomicrobia* was elevated (Fig. 5E,5G). Collectively, our data clearly indicated that HFD feeding resulted in a loss of microbial diversity and particularly increased the abundance of the *Firmicutes* phylum.

The pairwise Pearson correlations among all associated OTUs of the top 50 most abundant genera were visualized with a correlation network diagram, and all of the genera were from the phyla *Firmicutes*, *Bacteroidetes*, *Proteobacteria*, *Actinobacteria* and *Verrucomicrobia*. *Candidatus_Stoquefichus*, *Quinella*, *Ruminococcaceae_NK4A214_group*, *Clostridium_sensu_stricto_1* and *[Eubacterium]_fissicatena_group* from the *Firmicutes* phylum had the highest importance and the highest betweenness centrality within the NAFLD and Control network. This finding indicated that the changes in genus abundance of *Firmicutes* were most important in gut microbiota dysbiosis. The results of the 16S rRNA gene sequencing of the stool samples are shown in Fig. S2 and raw data of the 16S rRNA sequencing were deposited at SRA database of NCBI with the accession number SRP198883 and SRP198884.

3.6 Correlation of CA, HDCA or ωMCA with the gut microbiome in response to HFD feeding

With the help of the microbiota, BAs, including primary BAs, change markedly in the caecal content. As the top two most prevalent species in the liver BA pool, TCA and THDCA changed significantly in liver and serum samples. We hypothesized that they were converted into CA and HDCA, respectively, which made up the largest component of the BA caecal content pool. Tauro α-muricholic acid (TαMCA) and tauro β-muricholic acid (TβMCA) would be deconjugated into ωMCA by the gut

microbiota in the intestine. To provide a better understanding of the correlation of CA, HDCA or ωMCA with the gut microbiota, a Spearman correlation analysis was performed between the relative abundance of the differential microbial phylum or genus and the concentrations of these three BAs in the caecal content samples. To visualize the correlations of HDCA, ωMCA and CA, unsupervised clustering of OTUs to reveal different clusters of phyla or genera was first performed. HDCA was positively correlated with *Bacteroidetes*, which decreased in the NAFLD group. CA was positively correlated with *Firmicutes* and *Verrucomicrobia* and negatively correlated with *Bacteroidetes* (Fig. 6A).

Among the differential microbial genera shown in the heatmap, each had at least one significant correlation with a BA (Fig. 6B). Almost all of the microbes were significantly correlated with specific BAs. Thus, these microbes might be the bacteria that respond differentially to alterations in specific HFD-induced BA secretion. Through cluster analysis, the gut microbiome was categorized into three classes. Class G1 and most of Class G2 were negatively correlated with HDCA and ωMCA and were positively correlated with CA. The microbiome of Class G3 and part of Class G2 were positively correlated with HDCA and ωMCA and negatively correlated with CA. Considering the five top-ranked microbiome components related to BA based on the correlation coefficient and p value, it was shown that HDCA was closely positively correlated with *Ruminococcaceae_UCG-010*, *Peptococcus*, *Turicibacter*, and *norank_f__Bacteroidales_S24-7_group*, while it was negatively correlated with *unclassified_f__Christensenellaceae*. CA was closely positively correlated with *Staphylococcus, Actinomyces* and *Lachnospiraceae_UCG-010*, while it was negatively correlated with *[Eubacterium]_xylanophilum_group* and *Ruminiclostridium_6*. ωMCA was closely positively correlated with *Parasutterella*, *Tyzzerella*, *Intestinimonas*, *Lachnospiraceae_UCG-006* and *[Eubacterium]_brachy_group*. The correlation of CA, HDCA or ωMCA with the gut microbiome in the stool samples is shown in Fig. S3.

4. Discussion

BAs are amphipathic molecules that are produced in the liver using cholesterol as a raw material. Primary BAs can be synthesized via the classic (neutral) pathway and the alternative (acidic) pathway in the liver. After conjugation with glycine or taurine, BAs are excreted by hepatocytes into the canalicular space via the bile salt

export pump (BSEP or ABCB11) [33]. The bile containing BAs, free cholesterol and phospholipids is further released into the duodenum after a meal. The primary BAs are converted into secondary BAs by microbial modification in the gut. BAs are recirculated to the liver via the enterohepatic circulation by BA transporters or binding proteins (SLC10A2, ASBT, FABP6, IBABP, SLC51A/B, and OSTα/β located on ileal enterocytes and transporters on hepatocytes (NTCP or OATP)) [34].

Our present study showed the altered BA pool size and compositions in the serum, liver and caecal content after 18 weeks of high-fat diet feeding. The composition of TCA was increased, but THDCA was decreased in the liver. In the gut, the deconjugated form of TCA (CA) was increased, while the deconjugated form of THDCA (HDCA) was decreased. In the serum, the composition of TCA was increased, while both HDCA and tauro-conjugated HDCA (THDCA) were decreased. THDCA but not TCA induced the gene expression of apolipoprotein, bile secretion related proteins, and the Cytochrome P450 family, but suppressed inflammatory response gene expression in steatotic hepatocytes. As a result, THDCA ameliorated neutral lipid accumulation through activating FXR and improved insulin sensitivity in hepatocytes.

THDCA is a natural BA with hydrophilic properties that better stimulates cholesterol and phospholipid secretion into bile versus tauroursodeoxycholic acid (TUDCA) and TCA [35]. Considering THDCA's relatively high hydrophilicity, this BA has been proposed for the treatment of hepatic disorders. In the current study, we demonstrated that THDCA could ameliorate lipid accumulation through increased expression of apolipoprotein family and lipid metabolism genes and improve insulin sensitivity in a concentration-dependent manner in hepatocytes. As a FXR agonist, THDCA would reverse hepatic steatosis and protect against liver damage caused by HFD by stimulating FXR and its downstream target. In the NAFLD model, the composition of THDCA was decreased dramatically, which might be one of the reasons for lipid accumulation in the liver. We found a decreased composition of UDCA in the liver samples of the NAFLD group compared to the Control group. UDCA has been widely used to promote bile secretion in the clinic. UDCA and its taurine-conjugated variant could improve steatosis and inflammation in an animal model [36], while clinical studies showed that it significantly improved hepatic insulin resistance and glycaemic control but not histological improvement [36-38]. Of the natural FXR agonists, CDCA is the most potent endogenous activator, while LCA,

DCA and CA activate FXR with a moderate efficacy, with the conjugated forms being less potent [39]. Taken together, these data demonstrate that THDCA is a potentially potent FXR agonist in vivo.

TCA is the hydrophobic product of the conjugation of CA with taurine, which was found to downregulate gluconeogenic genes and induce proinflammatory gene expression in hepatocytes [40, 41]. TCA might be a potential biomarker of liver injury in rat toxicity studies [42]. Following treatment of rats with streptozotocin and high-fat diet, liver and plasma TCA were increased in all mice fed a HFD, and significantly more of those mice developed HCC versus controls [43]. Through bile acyl-CoA synthetase and bile acid-CoA, primary BAs are mainly conjugated to the amino acid taurine to form sodium salts with increased solubility in rodents [16, 44]. In fatty liver, due to increased synthesis of primary BAs, a large amount of CA is converted into TCA, which results in its increased proportion in the BA pool. Although TCA has been reported to improve insulin sensitivity and glucose metabolism through the ERK1/2 and AKT pathways, it would interfere with the secretion of VLDL particles [45-47]. Our results are in agreement with previous studies in the liver of human samples, reporting that the concentrations of TCA were significantly higher in the NAFLD group [24]. Based on transcriptome profiling and qRT-PCR, we found that TCA has a reduced effect on lipid metabolism and transportation and FXR activation versus THDCA.

Serum BAs would come from BAs absorbed in the portal or hepatic vein. The serum concentration of TCA was the only BA to be markedly higher in the NAFLD group, which was consistent with the observation that TCA was significantly higher in the plasma of patients with steatosis when compared to healthy people [48]. BA profiles in steatotic patients display similar changes to our high-fat diet fed rodent model. TCA was increased significantly in a diabetic mice model [49]. Similar to the changes in the liver, we found HDCA and THDCA to be decreased in serum samples in NAFLD. Serum TCA may be considered an indicator of NAFLD and a more sensitive and non-invasive diagnosis method.

Our results are in agreement with previous studies reporting that high-fat diet induced changes in intestinal flora including the increased abundance of *Firmicutes* and decreased abundance of *Bacteroidetes* [4, 23]. From our observation, *Bacteroidetes* is positively correlated with HDCA through deconjugation and

dihydroxylation of BAs. Previous research has shown that *Prevotella* was negatively correlated with CA [18]. Our results confirmed a similar correlation between *Prevotella_9* and CA. HDCA was positively correlated with *Ruminococcaceae_UCG-009*, *Ruminococcaceae_UCG-010* and *Ruminococcaceae_UCG-013*, which are genera from the *Firmicutes* phylum. In our study, we found that ωMCA was positively correlated with *Parasutterella*, *[Eubacterium]_brachy_group*. ωMCA was reported to be converted to βMCA through the oxidation of the *Eubacterium lentum* strain, so we further studied the species of the microbiota in the NAFLD model and identified relationships with BAs [50, 51].

The present study has several limitations, including the absence of information about the BA profile in the portal vein and a lack of intervention on the gut microbiota. Furthermore, the therapeutic effect of THDCA administration on an animal model of NAFLD requires further investigation. Additional studies about the relationship between BAs and the gut microbiome and whether THDCA could selectively eliminate bacteria or whether augmentation of specific gut microbiota would modify THDCA would be useful.

In conclusion, we reported the turnover of the BA profile in the serum, liver and caecal content in a rat NAFLD model. THDCA might improve hepatic steatosis in vitro through activating FXR. In addition, the altered BAs are highly correlated with gut dysbiosis.

5. Authors' contributions

YM and XL participated in the research design. JZ and YT conducted the animal experiments. XL, JL, CL and DX collected the data and performed the data analysis. XL, YT and YW contributed to the writing of the manuscript. All authors have read and approved the final manuscript.

6. Acknowledgment

The authors would like to thank Mr Qi Miao and Ms Jieting Tang for their help in manuscript preparation.

7. Fundings

This work was supported by the Major Project of National Twelfth Five Plan (2012ZX09303-001); the Major Project of National Thirteenth Five Plan (2017ZX09304016); the National Natural Science Foundation of China (NSFC 81670524, NSFC 31771308); the Shanghai Shenkang Hospital Development Center (16CR2009A); and Clinical Research Centre at Shanghai Jiao Tong University School of Medicine (DLY201607).

The funders had no role in the study design, data collection and analysis, decision to publish, or the preparation of the manuscript.

8. Conflict of interest

The authors declared that they had no conflicts of interest to this work.

Figure legend

Fig. 1 **Concentrations of BA species in serum, liver and caecal content were altered in the NAFLD rat model** (A) BAs in serum. (B) BAs in liver. (C) BAs in caecal content. The data are expressed as the mean ± SEM. *, $p < 0.05$, **, $p < 0.01$, ***, $p < 0.001$ vs. Control group.

Fig. 2 **Composition of BA species in serum, liver and caecal content were altered in the NAFLD rat model** (A) Changes in serum BA composition in the Control and NAFLD group. (B) The decreased composition of HDCA, muroCA, 6-keto-LCA, βDCA, and ωMCA and the increased composition of TCA among the BA pool in the serum from the HFD groups. (C) Changes in liver BA composition in Control and NAFLD group. (D) The decreased composition of THDCA, TωMCA, TDCA, TLCA, βDCA, 6keto-LCA, HDCA, LCA, NorDCA, muroCA, βCDCA, and UDCA and the increased composition of TCA among the BA pool in the liver of the HFD groups. (E) Changes in the caecal content BA composition in the Control and NAFLD group. (F)The increased composition of CA, GCA, CDCA, 3-DHCA, ACA, and NorCA and the decreased composition of ωMCA, HDCA, and muroCA among the BA pool in the caecal content of the HFD groups.*, $p < 0.05$, **, $p < 0.01$, ***, $p < 0.001$ vs. Control group.

Fig. 3 **Effects of THDCA and TCA on hepatic steatosis in vitro** (A) Hierarchical

clustering of BSA, OAPA, TCA and THDCA samples. (B) Diagram illustrating the genes that were upregulated and downregulated in the OAPA group compared to their expression in the BSA group. (C) Heatmap of different groups. (D) Diagram illustrating the genes that were upregulated and downregulated in the THDCA group or the TCA group compared to their expression in the OAPA group. (E) and (F) Significantly enriched biological process categories in the gene ontology (GO) analysis related to the genes that were upregulated (E) or downregulated (F) in the THDCA group compared to the expression levels in the OAPA group. (G) Heatmap of specific genes in the OAPA and THDCA groups. (H) Oil red O staining of BSA, OAPA and THDCA (250 μM) treatment and the quantification of the ratio relative to the results of the BSA group. (I) Protein levels of phospho-Akt-Ser473, total Akt, and beta-actin were observed by Western blot. Quantitative analysis of the Western blot for phospho-Akt-Ser473/Akt was conducted by ImageJ. *, $p< 0.05$, **, $p< 0.01$, ***, $p<0.001$.

Fig. 4 **THDCA ameliorated hepatic steatosis by activating FXR** (A) Hepatic mRNA levels of FXR in the Control group and the NAFLD group. (B) A dual luciferase reporter assay was performed to detect the effect of THDCA on FXR activity in BRL-3A cells. Data were normalized to Renilla luciferase activity and are presented as a relative fold change. (C) Oil red O staining of OAPA and OAPA+THDCA (250 μM) and OAPA+THDCA (250 μM)+Z-guggulsterone (Z-GG) treatment in BRL-3A cells and the quantification of the ratio relative to the results of the OAPA group. (D) mRNA levels of Ppargc1a, NTCP, Fkp5, Lpin1 and Cyp2c22 in the OAPA, OAPA+THDCA (250 μM) and OAPA+THDCA (250 μM)+Z-GG groups in BRL-3A cells. (E) Heatmap representing mRNA profiling analysis of all genes expressed in primary rat hepatocytes treated with OAPA and then treated with either Z-GG or various concentrations of BAs (THDCA, TCA) for 24 h. *, $p<0.05$ vs. OAPA group. #, $p<0.05$ vs. OAPA+THDCA (250 μM)+Z-GG group.

Fig. 5 **Analysis of the alterations in the gut microbiome composition in response to HFD feeding** (A) PCoA score plot based on Bray-Curtis metrics. (B) Unweighted UniFrac cluster tree based on Bray-Curtis metrics. (C) Relative abundances of the gut microbiota of each sample at the phylum level. (D) Wilcoxon rank-sum test bar plot at

the phylum level. (E) Relative abundances of the gut microbiota of each sample at the genus level. (F) Network analysis of caecal content 16S was performed at the genus level. The Spearman coefficient (r), ranging from positive (red) to negative (green) values, is reported (edges with $|r|>0.8$ with $p<0.01$). The edge thickness is proportional to the number of co-occurrences found between two nodes (species and species) linked by the edge itself. Bacterial species with a mean relative abundance in the top 50 are reported with their OTU number and are represented as circles. Node size is proportional to the number of edges departing from the node, indicating its degree of interaction. The node name size is proportional to the betweenness centrality, meaning the bridging/key importance of that node within the network. (G) Wilcoxon rank-sum test bar plot at the genus level.

Fig. 6 **Cross-correlation of the concentrations of CA, HDCA or ωMCA with the relative abundance of differential microbial phylum and genus** (A) The Spearman coefficient (r), ranging from positive (red) and negative (green) values, was used to cross-correlate the specific BAs HDCA, ωMCA and CA (within caecal sample) and the microbial phylum. (B) The Spearman coefficient (r), ranging from positive (red) and negative (green) values, was used to cross-correlate the specific BAs HDCA, ωMCA and CA (within caecal sample) and the microbial genus.

References

[1] Younossi ZM, Otgonsuren M, Henry L, Venkatesan C, Mishra A, Erario M, et al. Association of nonalcoholic fatty liver disease (NAFLD) with hepatocellular carcinoma (HCC) in the United States from 2004 to 2009. Hepatology. 2015;62:1723-30. https://doi.org/10.1002/hep.28123.

[2] Estes C, Razavi H, Loomba R, Younossi Z, Sanyal AJ. Modeling the epidemic of nonalcoholic fatty liver disease demonstrates an exponential increase in burden of disease. Hepatology. 2018;67:123-33. https://doi.org/10.1002/hep.29466.

[3] Musso G, Gambino R, Cassader M. Non-alcoholic fatty liver disease from pathogenesis to management: an update. Obes Rev. 2010;11:430-45. https://doi.org/10.1111/j.1467-789X.2009.00657.x.

[4] Loomba R, Seguritan V, Li W, Long T, Klitgord N, Bhatt A, et al. Gut Microbiome-Based Metagenomic Signature for Non-invasive Detection of Advanced Fibrosis in Human Nonalcoholic Fatty Liver Disease. Cell Metab. 2017;25:1054-62 e5. https://doi.org/10.1016/j.cmet.2017.04.001.

[5] Khan R, Bril F, Cusi K, Newsome PN. Modulation of Insulin Resistance in NAFLD. Hepatology. 2018. https://doi.org/10.1002/hep.30429.

[6] Lakhani HV, Sharma D, Dodrill MW, Nawab A, Sharma N, Cottrill CL, et al. Phenotypic Alteration of Hepatocytes in Non-Alcoholic Fatty Liver Disease. Int J Med Sci. 2018;15:1591-9. https://doi.org/10.7150/ijms.27953.

[7] Mazzoccoli G, De Cosmo S, Mazza T. The Biological Clock: A Pivotal Hub in Non-alcoholic Fatty Liver Disease Pathogenesis. Front Physiol. 2018;9:193. https://doi.org/10.3389/fphys.2018.00193.

[8] Yu Q, Jiang Z, Zhang L. Bile acid regulation: A novel therapeutic strategy in non-alcoholic fatty liver disease. Pharmacol Ther. 2018;190:81-90. https://doi.org/10.1016/j.pharmthera.2018.04.005.

[9] Marra F, Svegliati-Baroni G. Lipotoxicity and the gut-liver axis in NASH pathogenesis. J Hepatol. 2018;68:280-95. https://doi.org/10.1016/j.jhep.2017.11.014.

[10] Chu H, Duan Y, Yang L, Schnabl B. Small metabolites, possible big changes: a microbiota-centered view of non-alcoholic fatty liver disease. Gut. 2018. https://doi.org/10.1136/gutjnl-2018-316307.

[11] Trauner M, Fuchs CD, Halilbasic E, Paumgartner G. New therapeutic concepts in bile acid transport and signaling for management of cholestasis. Hepatology. 2017;65:1393-404. https://doi.org/10.1002/hep.28991.

[12] Hegyi P, Maleth J, Walters JR, Hofmann AF, Keely SJ. Guts and Gall: Bile Acids in Regulation of Intestinal Epithelial Function in Health and Disease. Physiol Rev. 2018;98:1983-2023. https://doi.org/10.1152/physrev.00054.2017.

[13] Singh M, Singh A, Kundu S, Bansal S, Bajaj A. Deciphering the role of charge, hydration, and hydrophobicity for cytotoxic activities and membrane interactions of bile acid based facial amphiphiles. Biochim Biophys Acta. 2013;1828:1926-37. https://doi.org/10.1016/j.bbamem.2013.04.003.

[14] Marin JJ, Macias RI, Briz O, Banales JM, Monte MJ. Bile Acids in Physiology, Pathology and Pharmacology. Curr Drug Metab. 2015;17:4-29.

[15] Halilbasic E, Claudel T, Trauner M. Bile acid transporters and regulatory nuclear receptors in the liver and beyond. J Hepatol. 2013;58:155-68. https://doi.org/10.1016/j.jhep.2012.08.002.

[16] Jia W, Xie G, Jia W. Bile acid-microbiota crosstalk in gastrointestinal inflammation and carcinogenesis. Nat Rev Gastroenterol Hepatol. 2018;15:111-28. https://doi.org/10.1038/nrgastro.2017.119.

[17] Wahlstrom A, Sayin SI, Marschall HU, Backhed F. Intestinal Crosstalk between Bile Acids and Microbiota and Its Impact on Host Metabolism. Cell Metab. 2016;24:41-50. https://doi.org/10.1016/j.cmet.2016.05.005.

[18] Zheng X, Huang F, Zhao A, Lei S, Zhang Y, Xie G, et al. Bile acid is a significant host factor shaping the gut microbiome of diet-induced obese mice. BMC Biol. 2017;15:120. https://doi.org/10.1186/s12915-017-0462-7.

[19] Begley M, Gahan CG, Hill C. The interaction between bacteria and bile. FEMS Microbiol Rev. 2005;29:625-51. https://doi.org/10.1016/j.femsre.2004.09.003.

[20] Chevre R, Silvestre-Roig C, Soehnlein O. Nutritional Modulation of Innate Immunity: The Fat-Bile-Gut Connection. Trends Endocrinol Metab. 2018;29:686-98. https://doi.org/10.1016/j.tem.2018.08.002.

[21] Sayin SI, Wahlstrom A, Felin J, Jantti S, Marschall HU, Bamberg K, et al. Gut microbiota regulates bile acid metabolism by reducing the levels of tauro-beta-muricholic acid, a naturally occurring FXR antagonist. Cell Metab. 2013;17:225-35. https://doi.org/10.1016/j.cmet.2013.01.003.

[22] Schneider KM, Albers S, Trautwein C. Role of bile acids in the gut-liver axis. J Hepatol. 2018;68:1083-5. https://doi.org/10.1016/j.jhep.2017.11.025.

[23] Boursier J, Mueller O, Barret M, Machado M, Fizanne L, Araujo-Perez F, et al. The severity of nonalcoholic fatty liver disease is associated with gut dysbiosis and shift in the metabolic function of the gut microbiota. Hepatology. 2016;63:764-75. https://doi.org/10.1002/hep.28356.

[24] Garcia-Canaveras JC, Donato MT, Castell JV, Lahoz A. A comprehensive untargeted metabonomic

analysis of human steatotic liver tissue by RP and HILIC chromatography coupled to mass spectrometry reveals important metabolic alterations. J Proteome Res. 2011;10:4825-34. https://doi.org/10.1021/pr200629p.

[25] Puri P, Daita K, Joyce A, Mirshahi F, Santhekadur PK, Cazanave S, et al. The presence and severity of nonalcoholic steatohepatitis is associated with specific changes in circulating bile acids. Hepatology. 2017. https://doi.org/10.1002/hep.29359.

[26] Jiao N, Baker SS, Chapa-Rodriguez A, Liu W, Nugent CA, Tsompana M, et al. Suppressed hepatic bile acid signalling despite elevated production of primary and secondary bile acids in NAFLD. Gut. 2018;67:1881-91. https://doi.org/10.1136/gutjnl-2017-314307.

[27] Mouzaki M, Wang AY, Bandsma R, Comelli EM, Arendt BM, Zhang L, et al. Bile Acids and Dysbiosis in Non-Alcoholic Fatty Liver Disease. PLoS One. 2016;11:e0151829. https://doi.org/10.1371/journal.pone.0151829.

[28] Xie G, Wang Y, Wang X, Zhao A, Chen T, Ni Y, et al. Profiling of serum bile acids in a healthy Chinese population using UPLC-MS/MS. J Proteome Res. 2015;14:850-9. https://doi.org/10.1021/pr500920q.

[29] Lan K, Su M, Xie G, Ferslew BC, Brouwer KL, Rajani C, et al. Key Role for the 12-Hydroxy Group in the Negative Ion Fragmentation of Unconjugated C24 Bile Acids. Anal Chem. 2016;88:7041-8. https://doi.org/10.1021/acs.analchem.6b00573.

[30] Conde de la Rosa L, Schoemaker MH, Vrenken TE, Buist-Homan M, Havinga R, Jansen PL, et al. Superoxide anions and hydrogen peroxide induce hepatocyte death by different mechanisms: involvement of JNK and ERK MAP kinases. J Hepatol. 2006;44:918-29. https://doi.org/10.1016/j.jhep.2005.07.034.

[31] Yang J, Dou Z, Peng X, Wang H, Shen T, Liu J, et al. Transcriptomics and proteomics analyses of anti-cancer mechanisms of TR35-An active fraction from Xinjiang Bactrian camel milk in esophageal carcinoma cell. Clin Nutr. 2018. https://doi.org/10.1016/j.clnu.2018.10.013.

[32] Wang Z, Yang X, Chen L, Zhi X, Lu H, Ning Y, et al. Upregulation of hydroxysteroid sulfotransferase 2B1b promotes hepatic oval cell proliferation by modulating oxysterol-induced LXR activation in a mouse model of liver injury. Arch Toxicol. 2017;91:271-87. https://doi.org/10.1007/s00204-016-1693-z.

[33] Wang Y, Ding WX, Li T. Cholesterol and bile acid-mediated regulation of autophagy in fatty liver diseases and atherosclerosis. Biochim Biophys Acta Mol Cell Biol Lipids. 2018;1863:726-33. https://doi.org/10.1016/j.bbalip.2018.04.005.

[34] Donkers JM, Roscam Abbing RLP, van de Graaf SFJ. Developments in bile salt based therapies: a critical overview. Biochem Pharmacol. 2018. https://doi.org/10.1016/j.bcp.2018.12.018.

[35] Loria P, Bozzoli M, Concari M, Guicciardi ME, Carubbi F, Bertolotti M, et al. Effect of taurohyodeoxycholic acid on biliary lipid secretion in humans. Hepatology. 1997;25:1306-14. https://doi.org/10.1002/hep.510250601.

[36] Mueller M, Thorell A, Claudel T, Jha P, Koefeler H, Lackner C, et al. Ursodeoxycholic acid exerts farnesoid X receptor-antagonistic effects on bile acid and lipid metabolism in morbid obesity. J Hepatol. 2015;62:1398-404. https://doi.org/10.1016/j.jhep.2014.12.034.

[37] Ratziu V, de Ledinghen V, Oberti F, Mathurin P, Wartelle-Bladou C, Renou C, et al. A randomized controlled trial of high-dose ursodesoxycholic acid for nonalcoholic steatohepatitis. J Hepatol. 2011;54:1011-9. https://doi.org/10.1016/j.jhep.2010.08.030.

[38] Kars M, Yang L, Gregor MF, Mohammed BS, Pietka TA, Finck BN, et al. Tauroursodeoxycholic Acid may improve liver and muscle but not adipose tissue insulin sensitivity in obese men and women.

Diabetes. 2010;59:1899-905. https://doi.org/10.2337/db10-0308.

[39] Porez G, Prawitt J, Gross B, Staels B. Bile acid receptors as targets for the treatment of dyslipidemia and cardiovascular disease. J Lipid Res. 2012;53:1723-37. https://doi.org/10.1194/jlr.R024794.

[40] Allen K, Jaeschke H, Copple BL. Bile acids induce inflammatory genes in hepatocytes: a novel mechanism of inflammation during obstructive cholestasis. Am J Pathol. 2011;178:175-86. https://doi.org/10.1016/j.ajpath.2010.11.026.

[41] Cao R, Cronk ZX, Zha W, Sun L, Wang X, Fang Y, et al. Bile acids regulate hepatic gluconeogenic genes and farnesoid X receptor via G(alpha)i-protein-coupled receptors and the AKT pathway. J Lipid Res. 2010;51:2234-44. https://doi.org/10.1194/jlr.M004929.

[42] Luo L, Schomaker S, Houle C, Aubrecht J, Colangelo JL. Evaluation of serum bile acid profiles as biomarkers of liver injury in rodents. Toxicol Sci. 2014;137:12-25. https://doi.org/10.1093/toxsci/kft221.

[43] Xie G, Wang X, Huang F, Zhao A, Chen W, Yan J, et al. Dysregulated hepatic bile acids collaboratively promote liver carcinogenesis. Int J Cancer. 2016;139:1764-75. https://doi.org/10.1002/ijc.30219.

[44] Li T, Chiang JY. Bile acid signaling in metabolic disease and drug therapy. Pharmacol Rev. 2014;66:948-83. https://doi.org/10.1124/pr.113.008201.

[45] Cheng Z, Liu G, Zhang X, Bi D, Hu S. Improvement of Glucose Metabolism Following Long-Term Taurocholic Acid Gavage in a Diabetic Rat Model. Med Sci Monit. 2018;24:7206-12. https://doi.org/10.12659/MSM.912429.

[46] Studer E, Zhou X, Zhao R, Wang Y, Takabe K, Nagahashi M, et al. Conjugated bile acids activate the sphingosine-1-phosphate receptor 2 in primary rodent hepatocytes. Hepatology. 2012;55:267-76. https://doi.org/10.1002/hep.24681.

[47] Lin Y, Havinga R, Verkade HJ, Moshage H, Slooff MJ, Vonk RJ, et al. Bile acids suppress the secretion of very-low-density lipoprotein by human hepatocytes in primary culture. Hepatology. 1996;23:218-28. https://doi.org/10.1002/hep.510230204.

[48] Kalhan SC, Guo L, Edmison J, Dasarathy S, McCullough AJ, Hanson RW, et al. Plasma metabolomic profile in nonalcoholic fatty liver disease. Metabolism. 2011;60:404-13. https://doi.org/10.1016/j.metabol.2010.03.006.

[49] Chen C, Hu B, Wu T, Zhang Y, Xu Y, Feng Y, et al. Bile acid profiles in diabetic (db/db) mice and their wild type littermates. J Pharm Biomed Anal. 2016;131:473-81. https://doi.org/10.1016/j.jpba.2016.09.023.

[50] Eyssen H, De Pauw G, Stragier J, Verhulst A. Cooperative formation of omega-muricholic acid by intestinal microorganisms. Appl Environ Microbiol. 1983;45:141-7.

[51] Ju T, Kong JY, Stothard P, Willing BP. Defining the role of Parasutterella, a previously uncharacterized member of the core gut microbiota. ISME J. 2019. https://doi.org/10.1038/s41396-019-0364-5.

Highlights

1. TCA was increased, but THDCA and UDCA were decreased in the liver of a rat NAFLD model.
2. CA was increased, while both HDCA and ωMCA were decreased in the caecal content of a rat NAFLD model.
3. TCA was increased, while both HDCA and THDCA were decreased in the serum of a rat NAFLD model.
4. THDCA might improve hepatic steatosis in vitro through activating FXR.
5. The altered bile acids were highly correlated with gut dysbiosis.

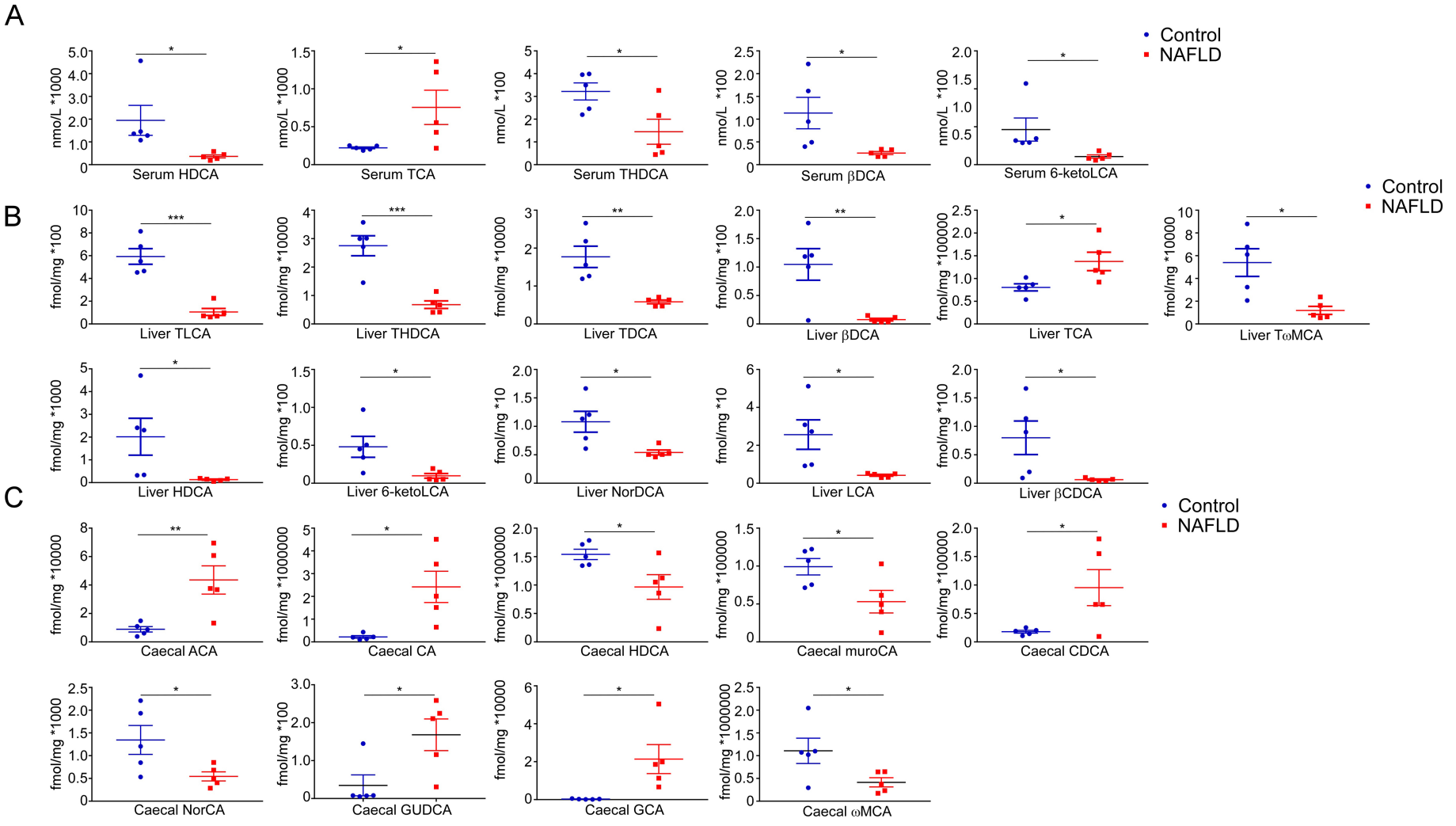
A
Control
NAFLD
nmol/L *1000
Serum HDCA
nmol/L *1000
Serum TCA
nmol/L *100
Serum THDCA
nmol/L *100
Serum βDCA
nmol/L *100
Serum 6-ketoLCA
B
Control
NAFLD
fmol/mg *100
Liver TLCA
fmol/mg *10000
Liver THDCA
fmol/mg *10000
Liver TDCA
fmol/mg *100
Liver βDCA
fmol/mg *100000
Liver TCA
fmol/mg *10000
Liver TωMCA
fmol/mg *1000
Liver HDCA
fmol/mg *100
Liver 6-ketoLCA
fmol/mg *10
Liver NorDCA
fmol/mg *10
Liver LCA
fmol/mg *100
Liver βCDCA
C
Control
NAFLD
fmol/mg *10000
Caecal ACA
fmol/mg *1000000
Caecal CA
fmol/mg *1000000
Caecal HDCA
fmol/mg *100000
Caecal muroCA
fmol/mg *100000
Caecal CDCA
fmol/mg *1000
Caecal NorCA
fmol/mg *100
Caecal GUDCA
fmol/mg *10000
Caecal GCA
fmol/mg *1000000
Caecal ωMCA

Figure 1

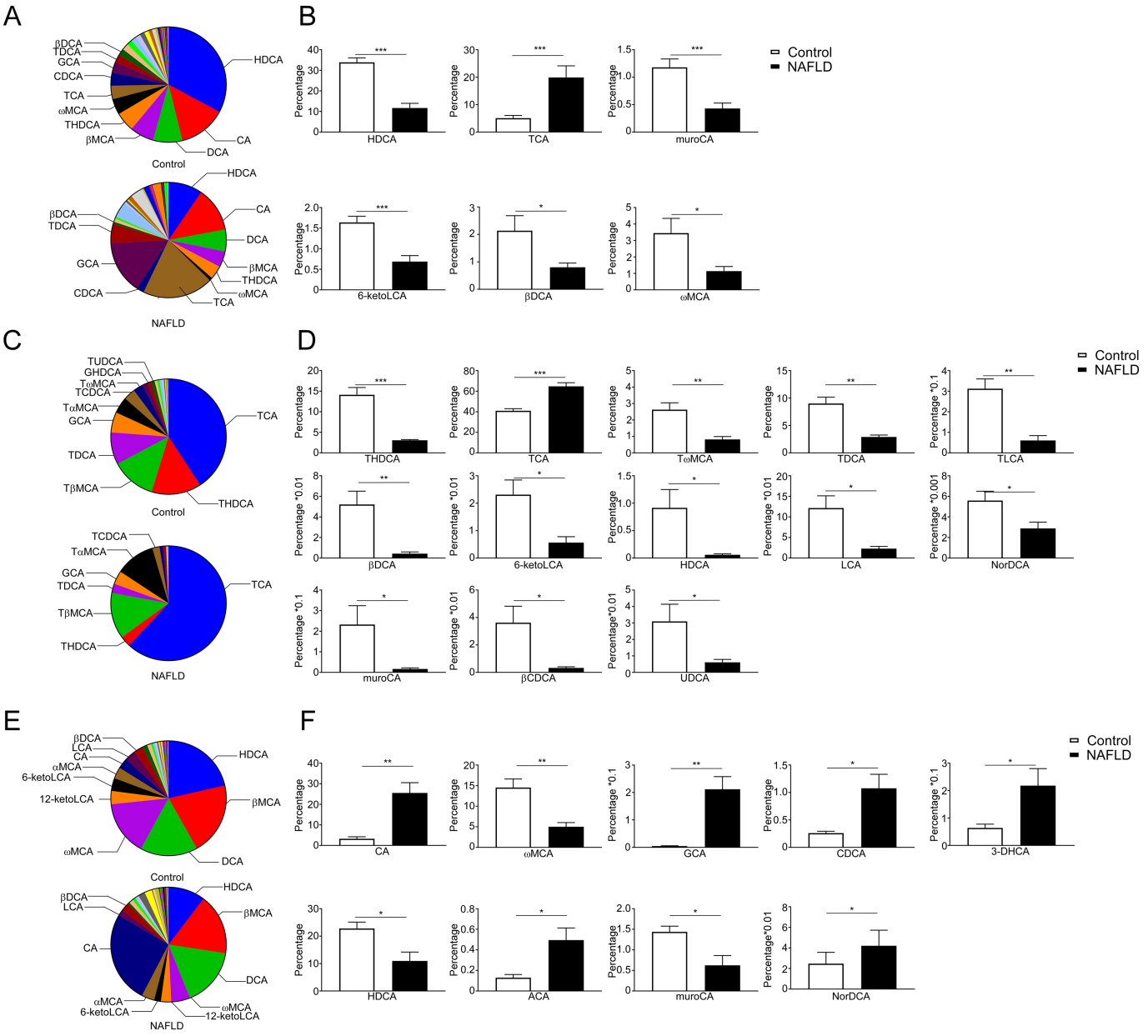
A
βDCA
TDCA
GCA
CDCA
TCA
ωMCA
THDCA
βMCA
HDCA
CA
DCA
Control
HDCA
CA
βDCA
TDCA
DCA
GCA
βMCA
THDCA
CDCA
ωMCA
TCA
NAFLD
B
Percentage
HDCA
TCA
muroCA
6-ketoLCA
βDCA
ωMCA
Control
NAFLD
C
TUDCA
GHDCA
TωMCA
TCDCA
TαMCA
GCA
TCA
TDCA
TβMCA
THDCA
Control
TCDCA
TαMCA
GCA
TDCA
TCA
TβMCA
THDCA
NAFLD
D
Percentage
THDCA
TCA
TωMCA
TDCA
TLCA
βDCA
6-ketoLCA
HDCA
LCA
NorDCA
muroCA
βCDCA
UDCA
Percentage *0.01
Percentage *0.1
Percentage *0.001
Control
NAFLD
E
βDCA
LCA
CA
αMCA
6-ketoLCA
12-ketoLCA
HDCA
βMCA
ωMCA
DCA
Control
HDCA
βDCA
LCA
βMCA
CA
DCA
αMCA
6-ketoLCA
ωMCA
12-ketoLCA
NAFLD
F
Percentage
CA
ωMCA
GCA
CDCA
3-DHCA
HDCA
ACA
muroCA
NorDCA
Percentage *0.1
Percentage*0.01
Control
NAFLD

Figure 2

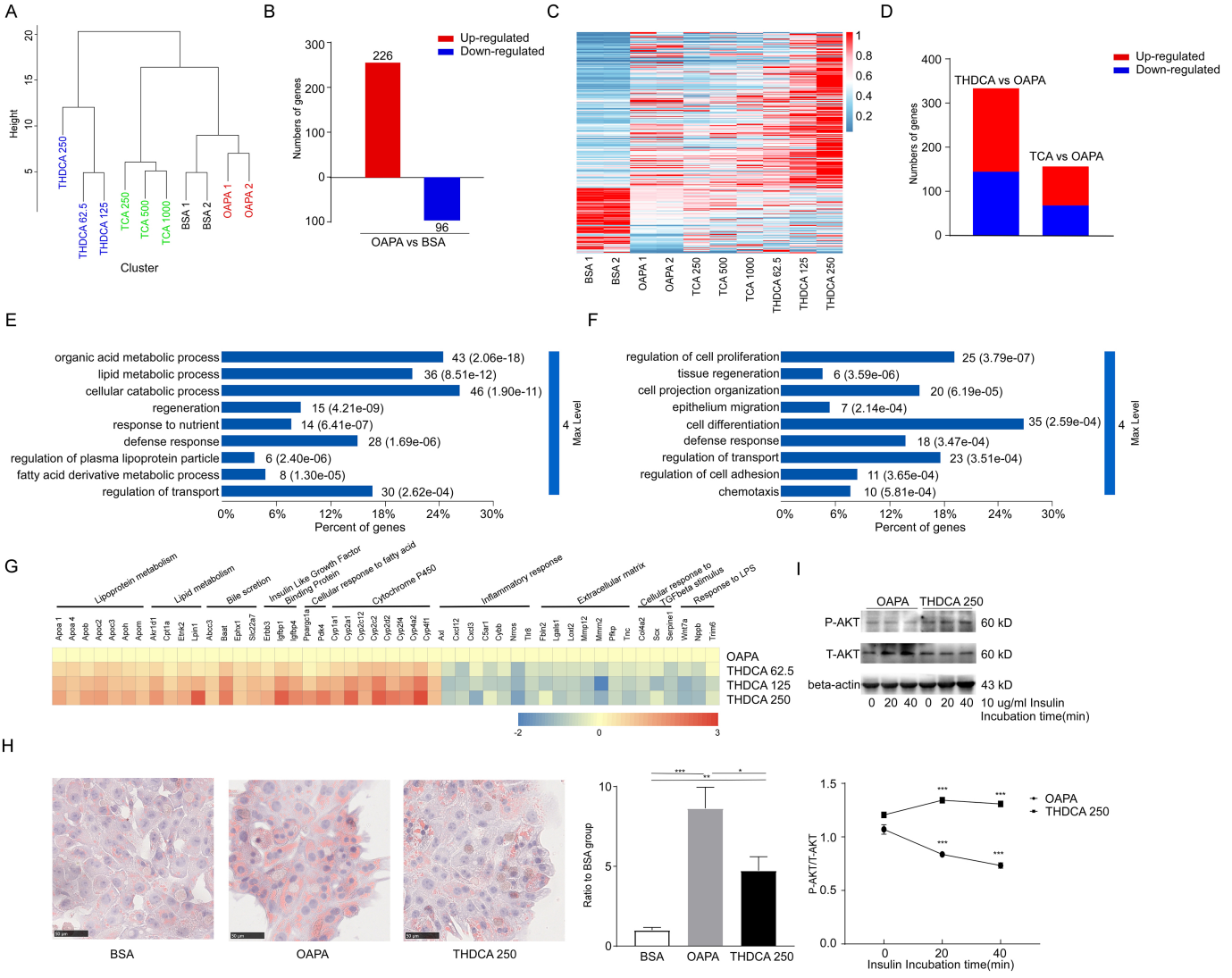
A
Height
20
15
10
5
THDCA 250
THDCA 62.5
THDCA 125
TCA 250
TCA 500
TCA 1000
BSA 1
BSA 2
OAPA 1
OAPA 2
Cluster
B
Up-regulated
Down-regulated
Numbers of genes
300
200
100
0
100
226
96
OAPA vs BSA
C
1
0.8
0.6
0.4
0.2
BSA 1
BSA 2
OAPA 1
OAPA 2
TCA 250
TCA 500
TCA 1000
THDCA 62.5
THDCA 125
THDCA 250
D
Up-regulated
Down-regulated
Numbers of genes
400
300
200
100
0
THDCA vs OAPA
TCA vs OAPA
E
organic acid metabolic process 43 (2.06e-18)
lipid metabolic process 36 (8.51e-12)
cellular catabolic process 46 (1.90e-11)
regeneration 15 (4.21e-09)
response to nutrient 14 (6.41e-07)
defense response 28 (1.69e-06)
regulation of plasma lipoprotein particle 6 (2.40e-06)
fatty acid derivative metabolic process 8 (1.30e-05)
regulation of transport 30 (2.62e-04)
4
Max Level
0%
6%
12%
18%
24%
30%
Percent of genes
F
regulation of cell proliferation 25 (3.79e-07)
tissue regeneration 6 (3.59e-06)
cell projection organization 20 (6.19e-05)
epithelium migration 7 (2.14e-04)
cell differentiation 35 (2.59e-04)
defense response 18 (3.47e-04)
regulation of transport 23 (3.51e-04)
regulation of cell adhesion 11 (3.65e-04)
chemotaxis 10 (5.81e-04)
4
Max Level
0%
6%
12%
18%
24%
30%
Percent of genes
G
Lipoprotein metabolism
Lipid metabolism
Bile scretion
Insulin Like Growth Factor Binding Protein
Cellular response to fatty acid
Cytochrome P450
Inflammatory response
Extracellular matrix
Cellular response to TGFbeta stimulus
Response to LPS
Apoa 1
Apoa 4
Apob
Apoc2
Apoc3
Apoh
Apom
Akr1d1
Cpt1a
Etnk2
Lpin1
Abcc3
Baat
Ephx1
Slc22a7
Erbb3
Igfbp1
Igfbp4
Ppargc1a
Pdk4
Cyp1a1
Cyp2a1
Cyp2c12
Cyp2c2
Cyp2d2
Cyp2j4
Cyp4a2
Cyp4f1
Axl
Cxcl12
Cxcl3
C5ar1
Cybb
Nrros
Tlr8
Fbln2
Lgals1
Loxl2
Mmp12
Mmp2
Prkp
Tnc
Col4a2
Scx
Serpine1
Wnt7a
Nppb
Timp6
OAPA
THDCA 62.5
THDCA 125
THDCA 250
-2
0
3
I
OAPA
THDCA 250
P-AKT
T-AKT
beta-actin
60 kD
60 kD
43 kD
0 20 40 0 20 40 10 ug/ml Insulin
Incubation time(min)
H
BSA
OAPA
THDCA 250
Ratio to BSA group
10
5
0
***
**
*
BSA
OAPA
THDCA 250
P-AKT/T-AKT
1.5
1.0
0.5
0.0
***
***
***
***
0
20
40
Insulin Incubation time(min)
OAPA
THDCA 250

Figure 3

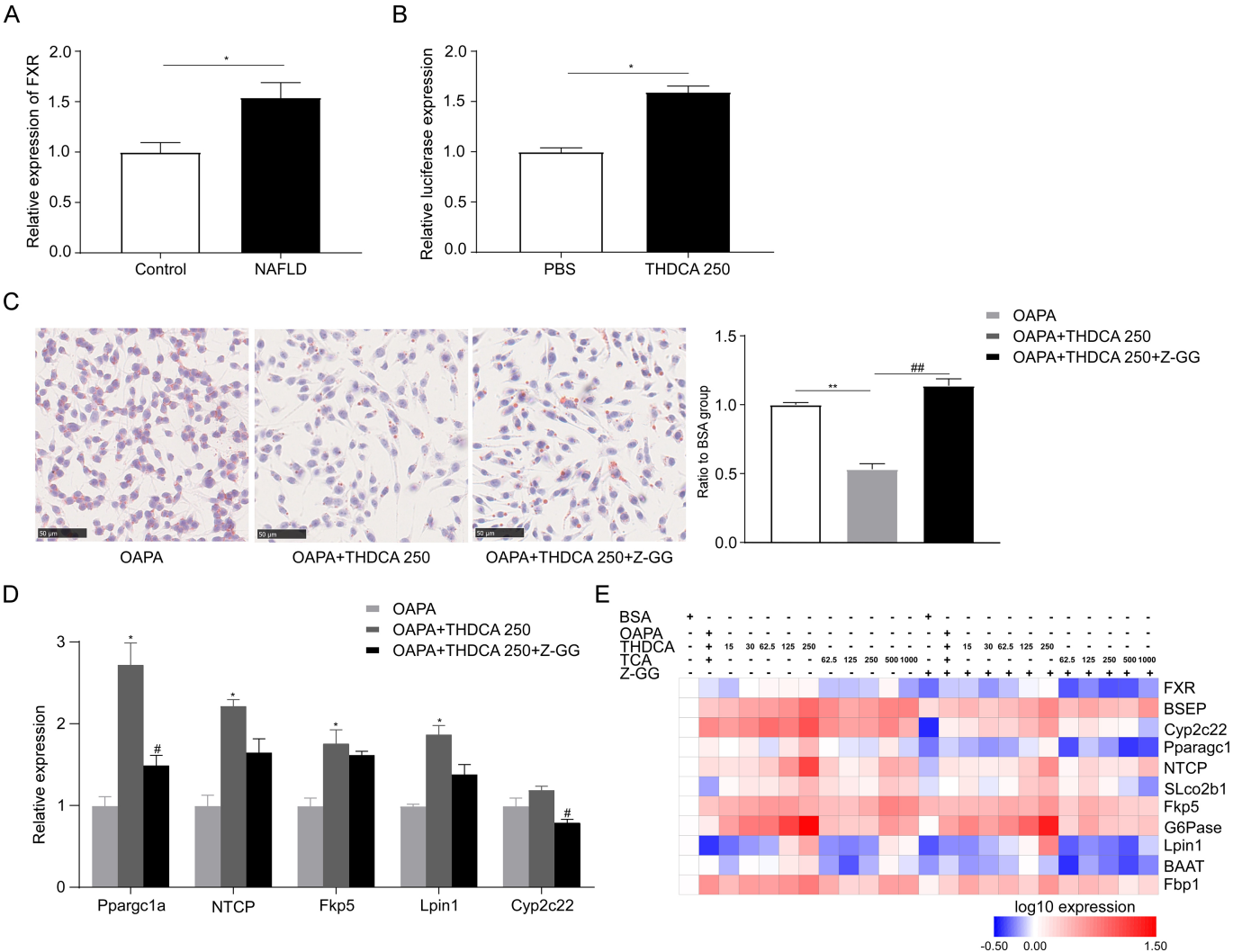
A
Relative expression of FXR
2.0
1.5
1.0
0.5
0.0
*
Control
NAFLD
B
Relative luciferase expression
2.0
1.5
1.0
0.5
0.0
*
PBS
THDCA 250
C
OAPA
OAPA+THDCA 250
OAPA+THDCA 250+Z-GG
50 μm
Ratio to BSA group
1.5
1.0
0.5
0.0
**
##
D
OAPA
OAPA+THDCA 250
OAPA+THDCA 250+Z-GG
Relative expression
3
2
1
0
Ppargc1a
NTCP
Fkp5
Lpin1
Cyp2c22
E
BSA
OAPA
THDCA
TCA
Z-GG
15 30 62.5 125 250
62.5 125 250 500 1000
FXR
BSEP
Cyp2c22
Pparagc1
NTCP
SLco2b1
Fkp5
G6Pase
Lpin1
BAAT
Fbp1
log10 expression
-0.50 0.00 1.50

Figure 4

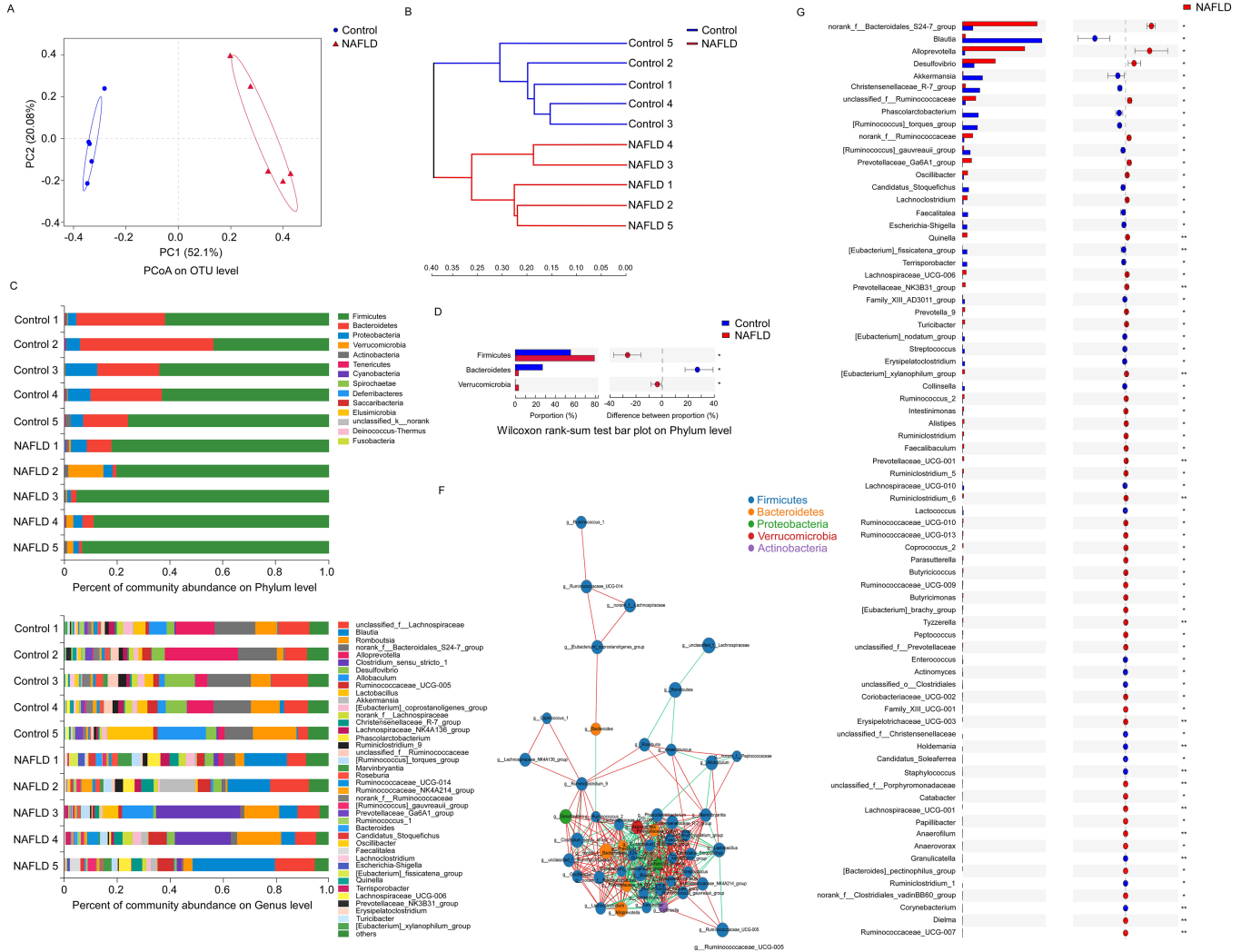
A
Control
NAFLD
PC2 (20.08%)
PC1 (52.1%)
PCoA on OTU level
B
Control
NAFLD
Control 5
Control 2
Control 1
Control 4
Control 3
NAFLD 4
NAFLD 3
NAFLD 1
NAFLD 2
NAFLD 5
C
Control 1
Control 2
Control 3
Control 4
Control 5
NAFLD 1
NAFLD 2
NAFLD 3
NAFLD 4
NAFLD 5
Firmicutes
Bacteroidetes
Proteobacteria
Verrucomicrobia
Actinobacteria
Tenericutes
Cyanobacteria
Spirochaetae
Deferribacteres
Saccharibacteria
Elusimicrobia
unclassified_k__norank
Deinococcus-Thermus
Fusobacteria
Percent of community abundance on Phylum level
D
Control
NAFLD
Firmicutes
Bacteroidetes
Verrucomicrobia
Porportion (%)
Difference between proportion (%)
Wilcoxon rank-sum test bar plot on Phylum level
E
unclassified_f__Lachnospiraceae
Blautia
Romboutsia
norank_f__Bacteroidales_S24-7_group
Alloprevotella
Clostridium_sensu_stricto_1
Desulfovibrio
Allobaculum
Ruminococcaceae_UCG-005
Lactobacillus
Akkermansia
[Eubacterium]_coprostanoligenes_group
norank_f__Lachnospiraceae
Christensenellaceae_R-7_group
Lachnospiraceae_NK4A136_group
Phascolarctobacterium
Ruminiclostridium_9
unclassified_f__Ruminococcaceae
[Ruminococcus]_torques_group
Marvinbryantia
Roseburia
Ruminococcaceae_UCG-014
Ruminococcaceae_NK4A214_group
norank_f__Ruminococcaceae
[Ruminococcus]_gauvreauii_group
Prevotellaceae_Ga6A1_group
Ruminococcus_1
Bacteroides
Candidatus_Stoquefichus
Oscillibacter
Faecalitalea
Lachnoclostridium
Escherichia-Shigella
[Eubacterium]_fissicatena_group
Quinella
Terrisporobacter
Lachnospiraceae_UCG-006
Prevotellaceae_NK3B31_group
Erysipelatoclostridium
Turicibacter
[Eubacterium]_xylanophilum_group
others
Percent of community abundance on Genus level
F
Firmicutes
Bacteroidetes
Proteobacteria
Verrucomicrobia
Actinobacteria
g__Ruminococcaceae_UCG-005
G
Control
NAFLD
norank_f__Bacteroidales_S24-7_group
Blautia
Alloprevotella
Desulfovibrio
Akkermansia
Christensenellaceae_R-7_group
unclassified_f__Ruminococcaceae
Phascolarctobacterium
[Ruminococcus]_torques_group
norank_f__Ruminococcaceae
[Ruminococcus]_gauvreauii_group
Prevotellaceae_Ga6A1_group
Oscillibacter
Candidatus_Stoquefichus
Lachnoclostridium
Faecalitalea
Escherichia-Shigella
Quinella
[Eubacterium]_fissicatena_group
Terrisporobacter
Lachnospiraceae_UCG-006
Prevotellaceae_NK3B31_group
Family_XIII_AD3011_group
Prevotella_9
Turicibacter
[Eubacterium]_nodatum_group
Streptococcus
Erysipelatoclostridium
[Eubacterium]_xylanophilum_group
Collinsella
Ruminococcus_2
Intestinimonas
Alistipes
Ruminiclostridium
Faecalibaculum
Prevotellaceae_UCG-001
Ruminiclostridium_5
Lachnospiraceae_UCG-010
Ruminiclostridium_6
Lactococcus
Ruminococcaceae_UCG-010
Ruminococcaceae_UCG-013
Coprococcus_2
Parasutterella
Butyricicoccus
Ruminococcaceae_UCG-009
Butyricimonas
[Eubacterium]_brachy_group
Tyzzerella
Peptococcus
unclassified_f__Prevotellaceae
Enterococcus
Actinomyces
unclassified_o__Clostridiales
Coriobacteriaceae_UCG-002
Family_XIII_UCG-001
Erysipelotrichaceae_UCG-003
unclassified_f__Christensenellaceae
Holdemania
Candidatus_Soleaferrea
Staphylococcus
unclassified_f__Porphyromonadaceae
Catabacter
Lachnospiraceae_UCG-001
Papillibacter
Anaerofilum
Anaerovorax
Granulicatella
[Bacteroides]_pectinophilus_group
Ruminiclostridium_1
norank_f__Clostridiales_vadinBB60_group
Corynebacterium
Dielma
Ruminococcaceae_UCG-007

Figure 5

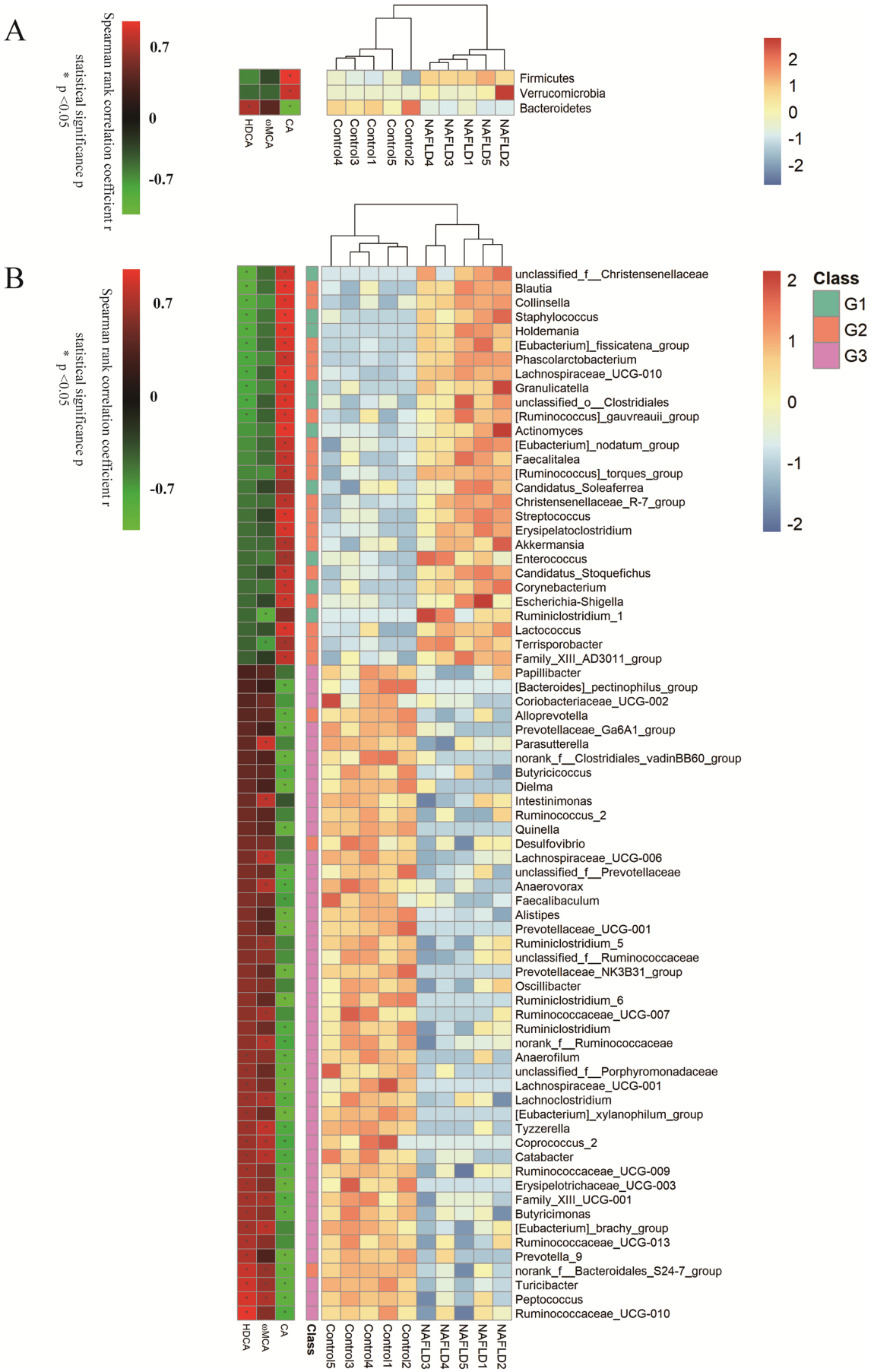
A
Spearman rank correlation coefficient r
0.7
0
-0.7
statistical significance p
* p <0.05
HDCA
oMCA
CA
Firmicutes
Verrucomicrobia
Bacteroidetes
Control4
Control3
Control1
Control5
Control2
NAFLD4
NAFLD3
NAFLD1
NAFLD5
NAFLD2
2
1
0
-1
-2
B
Spearman rank correlation coefficient r
0.7
0
-0.7
statistical significance p
* p <0.05
Class
G1
G2
G3
unclassified_f__Christensenellaceae
Blautia
Collinsella
Staphylococcus
Holdemania
[Eubacterium]_fissicatena_group
Phascolarctobacterium
Lachnospiraceae_UCG-010
Granulicatella
unclassified_o__Clostridiales
[Ruminococcus]_gauvreauii_group
Actinomyces
[Eubacterium]_nodatum_group
Faecalitalea
[Ruminococcus]_torques_group
Candidatus_Soleaferrea
Christensenellaceae_R-7_group
Streptococcus
Erysipelatoclostridium
Akkermansia
Enterococcus
Candidatus_Stoquefichus
Corynebacterium
Escherichia-Shigella
Ruminiclostridium_1
Lactococcus
Terrisporobacter
Family_XIII_AD3011_group
Papillibacter
[Bacteroides]_pectinophilus_group
Coriobacteriaceae_UCG-002
Alloprevotella
Prevotellaceae_Ga6A1_group
Parasutterella
norank_f__Clostridiales_vadinBB60_group
Butyricicoccus
Dielma
Intestinimonas
Ruminococcus_2
Quinella
Desulfovibrio
Lachnospiraceae_UCG-006
unclassified_f__Prevotellaceae
Anaerovorax
Faecalibaculum
Alistipes
Prevotellaceae_UCG-001
Ruminiclostridium_5
unclassified_f__Ruminococcaceae
Prevotellaceae_NK3B31_group
Oscillibacter
Ruminiclostridium_6
Ruminococcaceae_UCG-007
Ruminiclostridium
norank_f__Ruminococcaceae
Anaerofilum
unclassified_f__Porphyromonadaceae
Lachnospiraceae_UCG-001
Lachnoclostridium
[Eubacterium]_xylanophilum_group
Tyzzerella
Coprococcus_2
Catabacter
Ruminococcaceae_UCG-009
Erysipelotrichaceae_UCG-003
Family_XIII_UCG-001
Butyricimonas
[Eubacterium]_brachy_group
Ruminococcaceae_UCG-013
Prevotella_9
norank_f__Bacteroidales_S24-7_group
Turicibacter
Peptococcus
Ruminococcaceae_UCG-010
HDCA
oMCA
CA
Class
Control5
Control3
Control4
Control1
Control2
NAFLD3
NAFLD4
NAFLD5
NAFLD1
NAFLD2
2
1
0
-1
-2
Class
G1
G2
G3

Figure 6

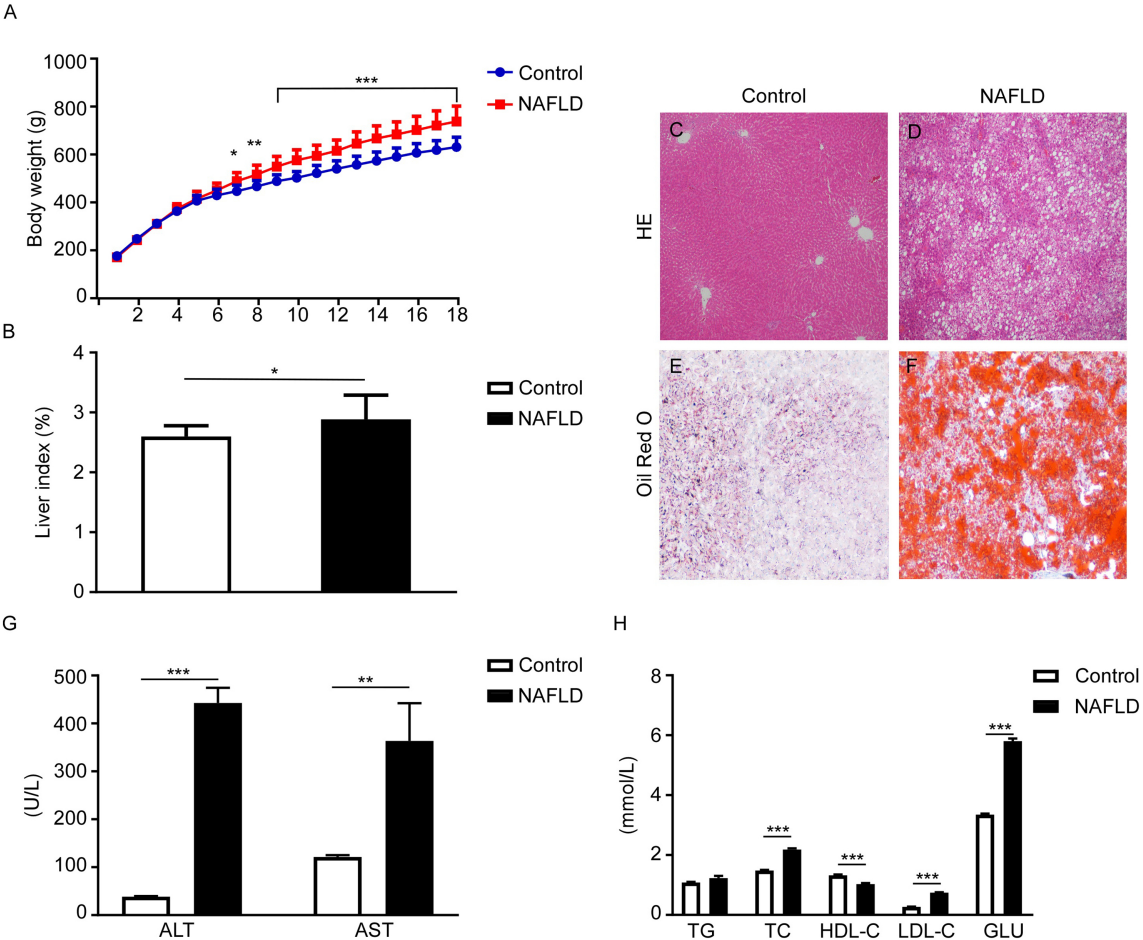
A
Body weight (g)
1000
800
600
400
200
0
2
4
6
8
10
12
14
16
18
*
**
***
Control
NAFLD
B
Liver index (%)
4
3
2
1
0
*
Control
NAFLD
Control
NAFLD
HE
Oil Red O
C
D
E
F
G
(U/L)
500
400
300
200
100
0
***
**
ALT
AST
Control
NAFLD
H
(mmol/L)
8
6
4
2
0
***
***
***
***
TG
TC
HDL-C
LDL-C
GLU
Control
NAFLD

Figure 7

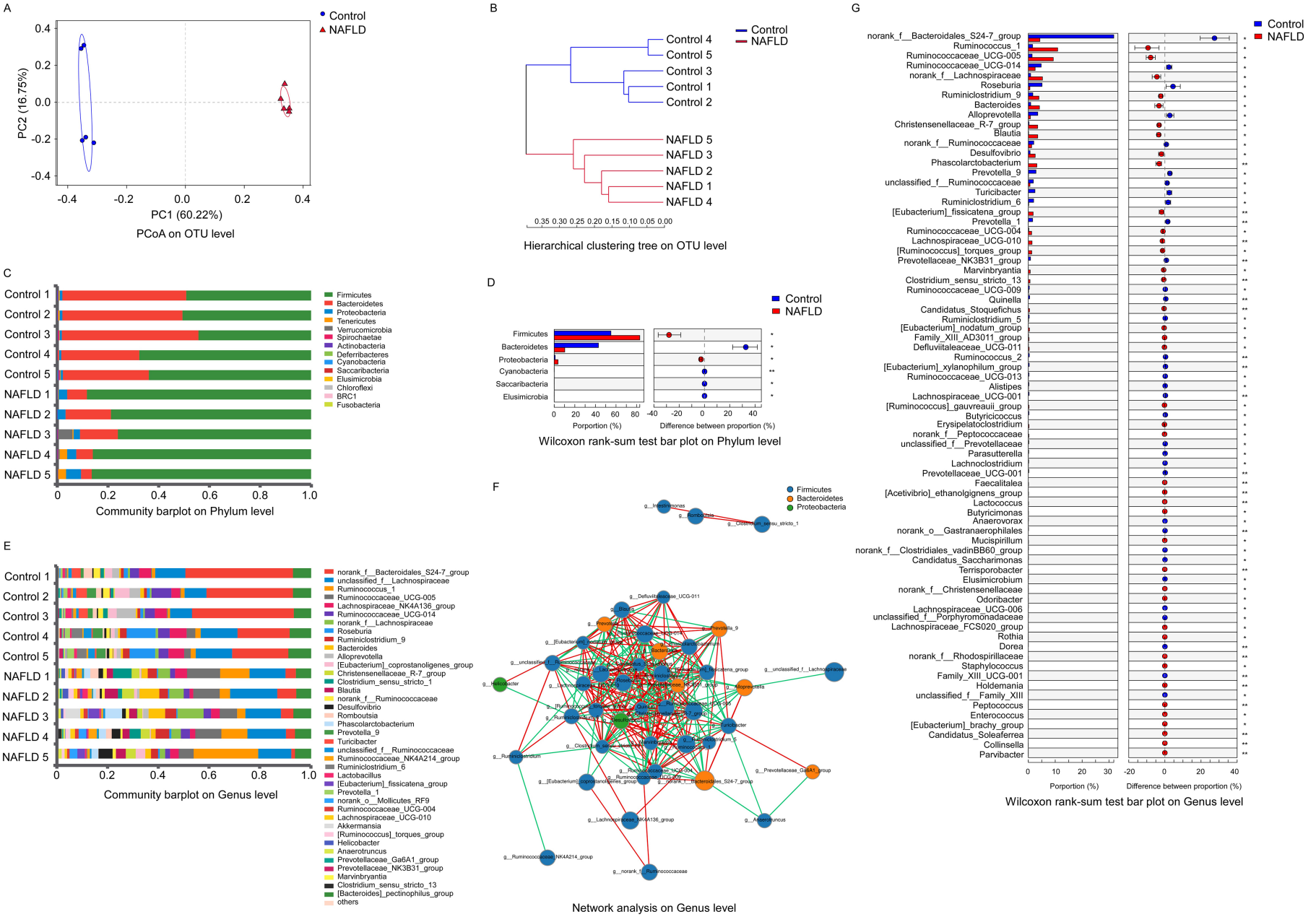
A
Control
NAFLD
PC2 (16.75%)
PC1 (60.22%)
PCoA on OTU level
B
Control
NAFLD
Control 4
Control 5
Control 3
Control 1
Control 2
NAFLD 5
NAFLD 3
NAFLD 2
NAFLD 1
NAFLD 4
Hierarchical clustering tree on OTU level
G
Control
NAFLD
norank_f__Bacteroidales_S24-7_group
Ruminococcus_1
Ruminococcaceae_UCG-005
Ruminococcaceae_UCG-014
norank_f__Lachnospiraceae
Roseburia
Ruminiclostridium_9
Bacteroides
Alloprevotella
Christensenellaceae_R-7_group
Blautia
norank_f__Ruminococcaceae
Desulfovibrio
Phascolarctobacterium
Prevotella_9
unclassified_f__Ruminococcaceae
Turicibacter
Ruminiclostridium_6
[Eubacterium]_fissicatena_group
Prevotella_1
Ruminococcaceae_UCG-004
Lachnospiraceae_UCG-010
[Ruminococcus]_torques_group
Prevotellaceae_NK3B31_group
Marvinbryantia
Clostridium_sensu_stricto_13
Ruminococcaceae_UCG-009
Quinella
Candidatus_Stoquefichus
Ruminiclostridium_5
[Eubacterium]_nodatum_group
Family_XIII_AD3011_group
Defluviitaleaceae_UCG-011
Ruminococcus_2
[Eubacterium]_xylanophilum_group
Ruminococcaceae_UCG-013
Alistipes
Lachnospiraceae_UCG-001
[Ruminococcus]_gauvreauii_group
Butyricicoccus
Erysipelatoclostridium
norank_f__Peptococcaceae
unclassified_f__Prevotellaceae
Parasutterella
Lachnoclostridium
Prevotellaceae_UCG-001
Faecalitalea
[Acetivibrio]_ethanolgignens_group
Lactococcus
Butyricimonas
Anaerovorax
norank_o__Gastranaerophilales
Mucispirillum
norank_f__Clostridiales_vadinBB60_group
Candidatus_Saccharimonas
Terrisporobacter
Elusimicrobium
norank_f__Christensenellaceae
Odoribacter
Lachnospiraceae_UCG-006
unclassified_f__Porphyromonadaceae
Lachnospiraceae_FCS020_group
Rothia
Dorea
norank_f__Rhodospirillaceae
Staphylococcus
Family_XIII_UCG-001
Holdemania
unclassified_f__Family_XIII
Peptococcus
Enterococcus
[Eubacterium]_brachy_group
Candidatus_Soleaferrea
Collinsella
Parvibacter
Porportion (%)
Difference between proportion (%)
Wilcoxon rank-sum test bar plot on Genus level
C
Control 1
Control 2
Control 3
Control 4
Control 5
NAFLD 1
NAFLD 2
NAFLD 3
NAFLD 4
NAFLD 5
Firmicutes
Bacteroidetes
Proteobacteria
Tenericutes
Verrucomicrobia
Spirochaetae
Actinobacteria
Deferribacteres
Cyanobacteria
Saccaribacteria
Elusimicrobia
Chloroflexi
BRC1
Fusobacteria
Community barplot on Phylum level
D
Control
NAFLD
Firmicutes
Bacteroidetes
Proteobacteria
Cyanobacteria
Saccaribacteria
Elusimicrobia
Porportion (%)
Difference between proportion (%)
Wilcoxon rank-sum test bar plot on Phylum level
E
Control 1
Control 2
Control 3
Control 4
Control 5
NAFLD 1
NAFLD 2
NAFLD 3
NAFLD 4
NAFLD 5
norank_f__Bacteroidales_S24-7_group
unclassified_f__Lachnospiraceae
Ruminococcus_1
Ruminococcaceae_UCG-005
Lachnospiraceae_NK4A136_group
Ruminococcaceae_UCG-014
norank_f__Lachnospiraceae
Roseburia
Ruminiclostridium_9
Bacteroides
Alloprevotella
[Eubacterium]_coprostanoligenes_group
Christensenellaceae_R-7_group
Clostridium_sensu_stricto_1
Blautia
norank_f__Ruminococcaceae
Desulfovibrio
Romboutsia
Phascolarctobacterium
Prevotella_9
Turicibacter
unclassified_f__Ruminococcaceae
Ruminococcaceae_NK4A214_group
Ruminiclostridium_6
Lactobacillus
[Eubacterium]_fissicatena_group
Prevotella_1
norank_o__Mollicutes_RF9
Ruminococcaceae_UCG-004
Lachnospiraceae_UCG-010
Akkermansia
[Ruminococcus]_torques_group
Helicobacter
Anaerotruncus
Prevotellaceae_Ga6A1_group
Prevotellaceae_NK3B31_group
Marvinbryantia
Clostridium_sensu_stricto_13
[Bacteroides]_pectinophilus_group
others
Community barplot on Genus level
F
Firmicutes
Bacteroidetes
Proteobacteria
Network analysis on Genus level

Figure 8


A
Spearman rank correlation coefficient r
0.7
0
-0.7
statistical significance p
* p <0.05
HDCA
ωMCA
CA
Class
Control 2
Control 1
Control 4
Control 3
Control 5
NAFLD 5
NAFLD 1
NAFLD 4
NAFLD 2
NAFLD 3
Firmicutes
Proteobacteria
Cyanobacteria
Bacteroidetes
Saccharibacteria
Elusimicrobia
Class
P1
P2
P3
B
Spearman rank correlation coefficient r
0.7
0
-0.7
statistical significance p
* p <0.05
Mucispirillum
Odoribacter
Bacteroides
Rothia
[Acetivibrio]_ethanolgignens_group
Lactococcus
Marvinbryantia
norank_f__Rhodospirillaceae
[Eubacterium]_fissicatena_group
Faecalitalea
Staphylococcus
norank_f__Lachnospiraceae
Phascolarctobacterium
[Ruminococcus]_gauvreauii_group
Blautia
Defluviitaleaceae_UCG-011
Erysipelatoclostridium
Christensenellaceae_R-7_group
Butyricimonas
Ruminococcus_1
Ruminococcaceae_UCG-005
Candidatus_Soleaferrea
Family_XIII_AD3011_group
Collinsella
Desulfovibrio
Candidatus_Stoquefichus
Ruminococcaceae_UCG-004
Parvibacter
Terrisporobacter
Ruminiclostridium_9
norank_f__Peptococcaceae
Enterococcus
[Ruminococcus]_torques_group
[Eubacterium]_nodatum_group
Holdemania
[Eubacterium]_brachy_group
Clostridium_sensu_stricto_13
norank_f__Christensenellaceae
Lachnospiraceae_FCS020_group
Lachnospiraceae_UCG-010
Peptococcus
Lachnoclostridium
norank_f__Ruminococcaceae
unclassified_f__Ruminococcaceae
unclassified_f__Family_XIII
Alloprevotella
Lachnospiraceae_UCG-006
unclassified_f__Prevotellaceae
Ruminiclostridium_6
Butyricicoccus
Parasutterella
Alistipes
Lachnospiraceae_UCG-001
Ruminococcus_2
Dorea
Family_XIII_UCG-001
Ruminiclostridium_5
Ruminococcaceae_UCG-014
[Eubacterium]_xylanophilum_group
Prevotellaceae_NK3B31_group
Quinella
Prevotella_9
Prevotella_1
norank_o__Gastranaerophilales
Roseburia
Candidatus_Saccharimonas
Turicibacter
norank_f__Bacteroidales_S24-7_group
Elusimicrobium
norank_f__Clostridiales_vadinBB60_group
Ruminococcaceae_UCG-009
unclassified_f__Porphyromonadaceae
Prevotellaceae_UCG-001
Ruminococcaceae_UCG-013
Anaerovorax
HDCA
ωMCA
CA
Class
Control 4
Control 5
Control 3
Control 1
Control 2
NAFLD 5
NAFLD 2
NAFLD 3
NAFLD 1
NAFLD 4
Class
G1
G2
G3
G4

Figure 9